Overlapping attentional networks yield divergent behavioral predictions across tasks: Neuromarkers for diffuse and focused attention?

Abbreviated title: Divergent predictions from attentional networks

Esther X.W. Wu[a,b], Gwenisha J. Liaw[b], Rui Zhe Goh[a], Tiffany T.Y. Chia[b], Alisia M.J. Chee[c], Takashi Obana[a,b,e], Monica D. Rosenberg[f], B.T. Thomas Yeo[b,c,d,g,h], & Christopher L. Asplund[a,b,d,e,g,h,*]

[a] Division of Social Sciences, Yale-NUS College, National University of Singapore, 16 College Ave West, Singapore 138527

[b] N.1 Institute for Health, National University of Singapore, 28 Medical Drive, #05-COR, Singapore 117456

[c] Department of Electrical and Computer Engineering, Faculty of Engineering, National University of Singapore, Block E4, Level 5, Room 42, 4 Engineering Drive 3, Singapore 117583

[d] Clinical Imaging Research Centre, Yong Loo Lin School of Medicine, 14 Medical Drive, #B1-01, Singapore 117599

[e] Department of Psychology, Faculty of Arts and Social Sciences, National University of Singapore, 5 Arts Link, Singapore, 117570

[f] Department of Psychology, University of Chicago, Chicago IL, USA 60637

[g] Centre for Cognitive Neuroscience, Duke-NUS Medical School, 8 College Road, Singapore 169857

[h] Institute for Application of Learning Science and Educational Technology, National University of Singapore, Singapore 119077

*To whom correspondence should be sent. Address: Yale-NUS College, 28 College Avenue West #01-501, Singapore 138533. Tel: +65 6601 3327. Email: chris.asplund@yale-nus.edu.sg.

Acknowledgements:

The authors would like to thank Mike Esterman for the GradCPT experiment and analysis code. This work was supported by grants from the Singapore Ministry of Defence, DSO National Laboratories, and Singapore Ministry of Education and Yale-NUS College start-up, all to Asplund. It was also supported by an NUS Cross-Faculty Research Grant to Yeo and Asplund. The authors have no conflicts of interest, financial or otherwise, with respect to their authorship or the publication of this article.

Number of pages for entire document (85), main text (52)

Number of figures (9), tables (3), multimedia (0) and 3D models (0)

Number of words for Abstract (250), Introduction (648), and Discussion (1497)

Abstract

Attention is a critical cognitive function, allowing humans to select, enhance, and sustain focus on information of behavioral relevance. Attention contains dissociable neural and psychological components. Nevertheless, some brain networks support multiple attentional functions. Connectome-based Predictive Models (CPM), which associate individual differences in task performance with functional connectivity patterns, provide a compelling example. A sustained attention network model (saCPM) successfully predicted performance for selective attention, inhibitory control, and reading recall tasks. Here we constructed a visual attentional blink (VAB) model (vabCPM), comparing its performance predictions and network edges associated with successful and unsuccessful behavior to the saCPM's. In the VAB, attention devoted to a target often causes a subsequent item to be missed. Although frequently attributed to attentional limitations, VAB deficits may attenuate when participants are distracted or deploy attention diffusely. Participants (n=73; 24 males) underwent fMRI while performing the VAB task and while resting. Outside the scanner, they completed other cognitive tasks over several days. A vabCPM constructed from these data successfully predicted VAB performance. Strikingly, the network edges that predicted better VAB performance (positive edges) predicted *worse* selective and sustained attention performance, and vice versa. Predictions from the saCPM mirrored these results, with the network's negative edges predicting better VAB performance. Furthermore, the vabCPM's positive edges significantly overlapped with the saCPM's negative edges, and vice versa. We conclude that these partially overlapping networks each have general attentional functions. They may indicate an individual's propensity to diffusely deploy attention, predicting better performance for some tasks and worse for others.

Significance statement

A longstanding question in psychology and neuroscience is whether we have general capacities or domain-specific ones. For such general capacities, what is the common function? Here we addressed these questions using the attentional blink (AB) task and neuroimaging. Individuals searched for two items in a stream of distracting items; the second item was often missed when it closely followed the first. How often the second item was missed varied across individuals, which was reflected in attention networks. Curiously, the networks' pattern of function that was good for the AB was bad for other tasks, and vice versa. We propose that these networks may represent not a general attentional ability, but rather the tendency to attend in a less focused manner.

Introduction

Attention is a critical cognitive function, allowing humans to select, enhance, and sustain focus on information of behavioral relevance. Visual attention plays numerous roles in different contexts, and it has been fractionated both behaviorally and neurally (Chun, Golomb, & Turk-Browne, 2011; Desimone & Duncan, 1995; Egeth & Yantis, 1997). In addition to such separable components, however, some brain networks support attentional processing across multiple domains (Asplund, Todd, Snyder, & Marois, 2010; Corbetta & Shulman, 2002; Duncan, 2010; Tamber-Rosenau, Dux, Tombu, Asplund, & Marois, 2013; Yeo, Krienen, et al., 2015). Recent studies using Connectome-based Predictive Models (CPM) support this idea. In a CPM approach, individual differences in behavioral performance are accounted for as a function of whole-brain functional connectivity patterns, after which performance for novel individuals can be predicted from fMRI data (Shen et al., 2017). Such predictions also apply across tasks. A sustained attention network model (saCPM) (Rosenberg, Finn, et al., 2016) could predict individual differences in performance for selective attention (Rosenberg, Hsu, Scheinost, Constable, & Chun, 2018), inhibitory control (Fountain-Zaragoza, Samimy, Rosenberg, & Prakash, 2019), and reading recall (Jangraw et al., 2018).

Here we constructed a CPM for the visual attentional blink (VAB), aiming to test whether that model could predict performance on a variety of tasks and to compare its predictions and network features to the saCPM's. In a VAB paradigm, participants search for two items in a stream of distractors; they often fail to perceive the second item, but only when it closely follows the first (200-500 ms) (Raymond, Shapiro, & Arnell, 1992). The VAB is critically dependent on attention, as no deficit occurs when the first item is ignored. Individuals differ in their VAB severity (rate of second item detection failures), and these differences are

typically large and stable (Dale, Dux, & Arnell, 2013). It is unclear, however, which cognitive and neural factors underlie them. Numerous theoretical explanations have been proposed for the VAB, including a temporary loss of control (Di Lollo, Kawahara, Shahab Ghorashi, & Enns, 2005) or bottleneck-like processing limitations (Chun & Potter, 1995). VAB magnitude also correlates only weakly with most other attention tasks (Skogsberg et al., 2015).

Intriguingly, VAB performance sometimes improves when attention to its primary detection task is reduced. Such reductions can be due to manipulation (Olivers & Nieuwenhuis, 2005, 2006) or dispositional factors (Dale & Arnell, 2010, 2015; Thomson, Ralph, Besner, & Smilek, 2015), and are thought to cause more diffuse attentional deployment. In particular, mind-wandering is associated with better VAB performance, though it has the opposite association for many other attention tasks (Gonçalves et al., 2017; Hu, He, & Xu, 2012; Robertson, Manly, Andrade, Baddeley, & Yiend, 1997; Smilek, Carriere, & Cheyne, 2010).

The VAB likely involves many factors (Dux & Marois, 2009), but which are reflected in individual differences of brain network function? To address this question using a CPM approach, we scanned 73 individuals while they performed the VAB task and while they rested. Resting state data allowed us to assess whether any predictive functional architecture persisted when participants were not engaged in attention-demanding tasks (Finn et al., 2015; Rosenberg, Finn, et al., 2016; Yoo et al., 2017). Outside the scanner, the same individuals completed cognitive tasks assessing sustained attention, selective attention, and fluid intelligence. We constructed a visual attentional blink CPM (vabCPM), from which we could make and assess predictions about the tasks. If attentional capacity predicts VAB performance, we would expect *positive* associations between vabCPM predictions for behavior and observed performance in other attention tasks. Conversely, if diffuse attentional tendencies predict VAB performance, we

might find significant *negative* associations between predicted and observed behavior for other attention tasks. For external validation, we made and assessed predictions about our tasks, including the VAB, using a sustained attention CPM (Rosenberg, Finn, et al., 2016). We then investigated and compared the networks associated with each model to better understand their relationship and potential psychological functions.

Materials and Methods

The present study included numerous tasks, with a primary focus on the visual attentional blink (VAB). Additional tasks provided critical context and points of comparison for understanding the individual differences in VAB performance and neural features. These additional tasks included those related to goal-directed attention and fluid intelligence. Many of these tasks are conceptually linked to the VAB (Dux & Marois, 2009), and many have also been studied themselves using Connectome-based Predictive Modeling (Finn et al., 2015; Rosenberg, Finn, et al., 2016; Rosenberg et al., 2018). To facilitate comparisons across these different tasks, we re-coded all behavioral performance measures such that positive numbers indicated better performance (e.g. higher accuracy or faster reaction times; see details below).

Experimental design

Participants. Eighty-two participants with self-reported normal or corrected-to-normal vision and normal hearing were recruited from the National University of Singapore (NUS) community. These individuals began a six-session study that included numerous behavioral and neuroimaging components, a subset of which are reported and analyzed here. Eight participants did not continue with the experiment after the first practice session (Session 0) and were excluded from the following analyses. One participant who did not achieve a target

142 discrimination score of 75% in the main VAB task (Session 1) was also excluded. Thus, unless
143 otherwise stated, the following analyses included data from 73 participants (24 males) between
144 the ages of 19-30 (M = 22.25, SD = 1.84). All participants provided written informed consent in
145 accordance with a protocol approved by the NUS Institutional Review Board and received
146 monetary compensation.

147 *Stimulus presentation.* All sessions took place either inside the MR scanner or in the
148 laboratory over a span of 3 weeks (see Table 1-1 of Extended Data for complete and detailed
149 experimental protocol). Inside the scanner, stimuli were presented at a viewing distance of 91 cm
150 on a 32-inch LCD monitor (NordicNeuroLab, Bergen, Norway) with a screen refresh rate of 60
151 Hz, connected to a MacBook Air (OS 10.12.1) running PyschoPy (Peirce, 2007). Participants
152 made responses using an MR-compatible button box. In the laboratory, stimuli were presented at
153 a distance of 57 cm on a 22-inch LCD monitor (Samsung SyncMaster 2233) with a screen
154 refresh rate of 60 Hz using an NVIDIA Quadro FX 3450/4000 SD graphics card on Windows 7.
155 Participants' responses were captured on a standard computer keyboard. Auditory stimuli were
156 presented using PyschoPy (Peirce, 2007) binaurally through Creative headphones.

157 *Overview of task domains and specific tasks*. The tasks in this study all investigated
158 cognitive processing, primarily different forms of attention (Table 1). Each task is detailed
159 below, organized by task domain. The task domains included the Attentional Blink, Sustained
160 Attention, Selective Attention, and Fluid Intelligence.

161

162 Table 1. Schedule of tasks and data used in analysis. Participants were encouraged to take breaks
163 between the tasks to prevent fatigue. With the exception of the Raven's Progressive Matrices
164 test, each task was performed twice on non-successive days. Task domains and tasks were as

follows. Attentional Blink: Visual Attentional Blink (VAB) and Auditory Attentional Blink (AAB). Sustained Attention: Visual Sustained Attention to Response Task (VSART), Auditory Sustained Attention to Response Task (ASART), and Gradual-onset Continuous Performance Task (GradCPT). Selective Attention: Attentional Network Task (ANT). Fluid Intelligence: Raven's Progressive Matrices test (Raven's).

Session	Days after previous session	Task	Data used in analysis
0	0	VAB (practice)	Behavior
1	3 to 14	Resting state	FMRI
		VAB (in scanner)	FMRI, Behavior
		ANT, VSART	Behavior
2	1	AAB, GradCPT, ASART	Behavior
3	1	ANT, VSART, Raven's	Behavior
4	1	AAB, GradCPT, ASART	Behavior
5	1 to 10	VAB (in scanner)	Behavior

Attentional Blink. Participants completed a visual attentional blink (VAB) and an auditory attentional blink (AAB) task. They were designed to be generally similar (Figure 1). Both versions were built around target discrimination and a probe detection, with each item embedded within a stream of distractors. Our main task of interest is the VAB, for which neuroimaging data was collected concurrently. For the AAB and all other tasks, only behavioral data were collected.

178

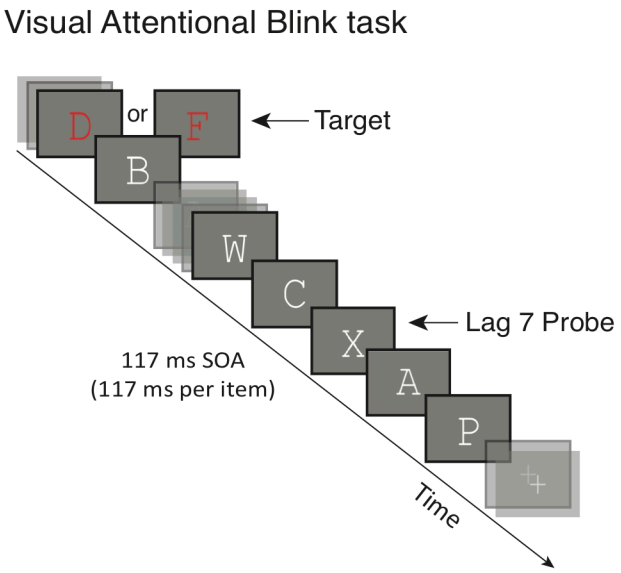

179

180 Figure 1. Experimental paradigm for the visual attentional blink (VAB) task. Participants
181 identified a target and then detected a probe within a stream of distractors, responding when
182 prompted at the conclusion of the stream. The target was a red letter, the probe was a white letter
183 X, and distractors were other white letters. The auditory attentional blink (AAB) task was
184 similar, save targets were complex tones, the probe was a high-pitched pure tone, and distractors
185 were other pure tones. SOA = stimulus onset asynchrony.

186

187 For the VAB, stimuli consisted of upper-case letters presented in Courier New Font on a
188 dark gray background (Figure 1). Targets were red letters D or F, whereas the probe was a white
189 letter X. Distractors were white letters save D, F, X, I, L, O, and Q. Targets and probes were
190 embedded within a rapid serial presentation stream, with no items repeated during each trial. The
191 stimulus onset asynchrony (SOA) between successive items in the 16-stimulus stream was 117
192 ms (no gap). A target appeared during every trial at serial position 3, 4, or 5, whereas the probe
193 appeared during 75% of trials. When present, the probe appeared at lags 1, 2, 3, 5, 7, or 9 relative

to the target, with the same number of trials per lag condition in each block. The first three lags were expected to be within the AB window, whereas the last three were expected to be outside it. In a small percentage of trials (14%), an irrelevant surprise stimulus (randomly selected from a set of 24 grayscale male faces and 24 colorful objects) was presented at lags 2 or 6 relative to the target. These surprise stimuli are not relevant to this current study; trials containing surprises were excluded from the following analyses and are not reported further.

Each 6.25-second trial began with the presentation of a white fixation cross (0.8° x 0.8°) for 500 ms, which became larger (1.0° x 1.0°) and turned yellow to signify that the rapid serial visual presentation (RSVP) stream would begin in 750 ms. Participants searched this RSVP stream (1867 ms) for the target and probe, which they then indicated by button box press after a blank gap (233 ms) at the trial's conclusion. A maximum of 2.9 s was given for participants to respond to both the target and probe response prompts. After this period, no further responses were recorded and the white fixation cross returned until the start of the next trial. Failure to respond was rare: No session had more than 0.16% no-target response trials or 0.64% no-probe response trials averaged across participants, and no participant had more than 3.57% (target) or 4.17% (probe) no-response trials in any given session. The timing between each trial was optimized for functional Magnetic Resonance Imaging (fMRI). As such, it followed an exponential distribution with a range of 1.25-10 s and mean of 3.75 s. Each session contained six blocks of 28 trials each, with the trials presented in a pseudorandom order. The 168 trials took approximately 40 minutes to complete, including breaks. Before the main experimental blocks in each session, each participant completed 3 practice blocks of 8 trials each. The first block contained targets but no probes; the second block contained probes but no targets; and the third block contained both.

For the AAB, targets were low-pitched or high-pitched complex tones comprised of five log-related frequencies (794 to 1260 Hz, or 1349 to 2142 Hz), whereas the probe was a 4000 Hz pure tone. Distractors were 19 pure tones of log-related frequencies ranging from 697 to 2911 Hz. Sound stimuli were adjusted to have equal mean absolute amplitudes, after which the probe and distractor intensities were set to 45% and 30% of the target intensity (~70 dB). These values were based on performance in Obana, Lim, & Asplund (under review) and additional pilot tests. As in the visual task, a small percentage of auditory trials (14%) contained an irrelevant surprise stimulus, randomly selected from a set of 24 sounds (including an alarm, a cough, and spoken letters), presented at lags 2 or 6 relative to the target. Again, surprise trials were not analyzed here. With the exception of a change in stimuli, trial structure was identical to the VAB.

Each 6.25-second trial began with a reminder of the target and probe sounds, which were played for 110 ms each with a gap of 85 ms. After 750 ms, the rapid auditory stream (RAP) began, through which participants searched for the target and probe. Similar to the visual task, the identity of the target and the presence of the probe were indicated by keypress after a blank gap (233 ms). Response prompts for the target and probe then appeared, with a maximum allowed time of 2.9 s for both responses. The timing between each trial was fixed at 0.75 s. Except for the blank gap and the response prompts, a white fixation cross (0.8° x 0.8°) was shown on the screen throughout the block. Each session contained three blocks of 56 trials each, with the trials presented in a pseudorandom order. The 168 trials took approximately 25 minutes to complete, including breaks. Before the main experimental blocks in each session, each participant completed 3 practice blocks of 8 trials each. The first block contained targets but no probes; the second block contained probes but no targets; and the third block contained both.

239 Before beginning each practice and task block of the auditory task, participants could play the
240 target and probe sounds as many times as desired.

241 *Sustained attention.* To better understand VAB performance in relation to other forms of
242 attention and their neural underpinnings, we also ran three sustained attention tasks. These
243 paradigms included the visual and auditory versions of the Sustained Attention to Response Task
244 (SART; Robertson, Manly, Andrade, Baddeley, & Yiend, 1997), which we adapted from Seli,
245 Cheyne, Barton, & Smilek (2012), and the Gradual-Onset Continuous Performance Task
246 (GradCPT; Esterman, Noonan, Rosenberg, & DeGutis, 2013; Rosenberg, Noonan, DeGutis, &
247 Esterman, 2013). The SART has been frequently used to examine moment-to-moment
248 fluctuations of sustained attention, requiring participants to make continuous responses to most
249 stimuli but withhold responses to a few. However, due to its trial-based structure, which may
250 provide a short 'break' between trials and not tax attention sufficiently, the GradCPT was later
251 designed to present images that gradually transition from one to the next using a linear pixel-by-
252 pixel interpolation. The GradCPT has been shown to show reliable and large interindividual
253 variability amongst high-functioning young adults, such as those in our sample (Rosenberg,
254 Finn, et al., 2016; Rosenberg et al., 2013).

255 In the VSART, participants were presented single digits, one after another, in the center
256 of the display screen. They were asked to press the spacebar if they saw a number from 1 to 9,
257 but withhold their response if they saw the number 3. Each digit was presented for 250 ms,
258 followed by an encircled "x" mask for 900 ms. Digits were presented in Symbol font in white,
259 against a black background, at sizes 0.57^{o}, 1.03^{o}, 1.43^{o}, 1.89^{o}, 2.35^{o} of visual angle. The order of
260 the digits and their sizes were randomized. Participants completed 675 trials (~ 13.5 mins) in
261 each session.

For the ASART, stimuli consisted of spoken single numbers. As in the visual task, participants were asked to press the spacebar when they heard the numbers 1 to 9, but to withhold their response if they heard the number 3. The numbers were presented in random order, each for 250 ms, following by a pink noise mask of 900 ms. Throughout the experiment, participants maintained fixation on a cross in the middle of the display. Each session consisted of 675 trials (~13.5 mins).

The GradCPT (Rosenberg et al., 2013) consisted of images that gradually transitioned from one to the next using a linear pixel-by-pixel interpolation (ISI = 800 ms). Images consisted of 10 mountain and 10 city scenes, randomly presented with 10% and 90% probability, respectively, without repeats in consecutive images. Participants were instructed to press the spacebar when a city scene was presented, but to withhold their response when a mountain scene was presented. To tax sustained attention sufficiently, the GradCPT was performed in a single block over a relatively long duration (15 min).

Selective attention. To understand the AB's relationship to other selective attention tasks and their neural underpinnings, we also employed the Attentional Network Task (ANT), by Fan, McCandliss, Sommer, Raz, & Posner (2002). This paradigm was designed to test three separable components of selective attention: alerting, orienting and executive control (Posner & Petersen, 1990) within a single experimental session. Stimuli consisted of 5 black lines (some with arrowheads) arranged horizontally in a row, against a grey background. The target, always an arrow in the center, was flanked on each side by (i) two arrows pointing in the same direction as the target (congruent condition), (ii) two arrows pointing in the opposite direction from the target (incongruent condition), or (iii) two black lines without arrowheads (neutral condition). Each line or arrow measured 0.55° horizontally, and the space between two adjacent objects measured

0.06°. To trigger attention orienting, all stimuli were presented either 1.06° above or below a central fixation cross. Participants were asked to keep their eyes fixated on the fixation cross and respond whether the target was pointing right or left.

Each trial started with a central fixation cross (400 – 1600 ms), followed by a warning cue (100 ms), a second central fixation cross (400 ms), and finally, the stimuli consisting of target and flankers presented either above or below a central fixation cross. Target and flankers were presented for 1700 ms, or until a response was made, whichever was shorter. A fixation cross was then presented until the end of trial (4000 ms after the first fixation period). For the warning cue, four types of cues were presented: (i) no cue (a central fixation cross, similar to that presented during the first and second fixation period, was presented), (ii) a center cue (an asterisk was presented in the center, thus alerting the participant to the impending stimuli presentation), (iii) double cue (two asterisks were presented above and below a central fixation cross, at both possible locations of the target), and (iv) a spatial cue (an asterisk was presented at the impending location of the target). Participants completed 3 blocks of 96 trials (4 cue conditions x 2 target locations x 2 target directions x 2 repetitions), with trials presented in random order. The entire task lasted about 30 min.

Fluid intelligence. As a final comparison domain for understanding VAB performance and the associated neural underpinnings, we measured fluid intelligence. Participants completed a shortened, nine-item version (Form A; Bilker et al., 2012) of the original 60-item Raven's Standard Progressive Matrices (Raven, Raven, & Court, 1998). The task was completed on a laboratory computer, and there were no response time limits. The task consists of pattern matching questions designed to measure abstract reasoning skills, and it has been typically used in clinical settings as a non-verbal test of fluid intelligence.

Statistical analyses for behavioral data

Participants had to meet a minimum target discrimination (letter D or F?) score of 75% for the VAB and 60% for the AAB to be included in the final sample. As a result, 73 sets of data were available for all tasks, with the exception of the AAB task (n=71). For the AAB, two additional participants were excluded because their target discrimination performance did not meet the minimum threshold in each session. For all behavioral comparisons, *p*-values were based on two-tailed comparisons. We also did not correct any behavioral comparisons for multiple corrections, as we wanted to find any normality violations and used the task correlations to identify any relationships that might affect our CPM results.

The computation of each behavioral measure is detailed in the following sections, again organized by task domain. To obtain stable behavioral metrics, we computed a 'best score' for each task metric. When data was available across two different sessions, the final score was averaged across both sessions. (When data was available only from a single session, the final score set to that session's.) We assessed whether the distribution of 'best scores' for each metric departed from normality using Jarque-Bera tests. As many normality violations were found, we used Spearman correlations of the 'best scores' to compare each pair of tasks. For tasks with two sessions, we also calculated test-retest reliability. Due to the aforementioned normality violations, Spearman correlations were again used.

Attentional blink. The VAB and AAB deficits were calculated in the same way. For each participant, we first computed the mean probe detection accuracy for each lag condition, contingent upon correct identification of the target. Probe detection accuracy scores were then averaged across short-lag (lags 1, 2, or 3) and long-lag (lags 5, 7, 9) conditions. The former condition was expected to be within the attentional blink window, whereas the latter condition

was expected to be outside it. The AB deficit was computed by regressing out the long-lag scores from the short-lag scores of each participant (short-lag scores ~ long-lag scores), and then saving the residuals (MacLean & Arnell, 2012). Larger and positive values indicated smaller attentional deficits, and thus better task performance. Note that simply subtracting the short-lag from the long-lag scores yielded highly similar VAB deficit scores ($r(71) = .955$). Visual AB scores (VABresid) were obtained from sessions 1 and 5, and the auditory AB scores (AABresid) were obtained from sessions 2 and 4.

Sustained attention. D-prime values were computed for the VSART, ASART and GradCPT, with larger values indicative of better performance in sustained attention. VSART scores (VSARTdprime) were obtained from sessions 1 and 3, ASART scores (ASARTdprime) were obtained from sessions 2 and 4, and GradCPT scores (GradCPTdprime) were obtained from sessions 2 and 4.

Selective attention. To measure overall task performance in the ANT task, we computed the mean error rate (ANTerr) across all trials and the intra-individual variability of RTs (ANTrtvar) for each participant. Intra-individual RT variability was computed as the standard deviation divided by mean of correct-trial RTs. Arguably, this metric is a more sensitive measure of task performance than mean error rate (Rosenberg et al., 2018; Wojtowicz, Berrigan, & Fisk, 2012), with higher RT variability being linked to lower accuracy in ANT tasks (Adolfsdottir, Sorensen, & Lundervold, 2008; Lundervold et al., 2011).

We also calculated metrics for each attentional network in the ANT, which putatively reflect their efficiencies. To do so, we compared the RTs between different trial conditions for each participant (Fan et al., 2002; Rosenberg et al., 2018). For the alerting network, efficiency was computed by subtracting the mean RT of double-cue condition from the mean RT of the no-

354 cue condition (ANTaert). Larger values would indicate faster responses due to the cue and thus
355 better task performance. For the orienting network, efficiency was computed by subtracting the
356 mean RT of spatial-cue condition from the mean RT of the center-cue condition (ANToert), thus
357 larger positive values would also imply faster responses due to the cue and better task
358 performance. For the executive control network, efficiency was computed by subtracting the
359 mean RT of the congruent condition from the mean RT of the incongruent condition (ANTcert).
360 In this case, smaller values would imply less interference by the flanker arrows and better task
361 performance. For all computations of efficiency with RTs, only trials with correct responses
362 were included.

363 For easier comparisons with the other behavioral measures, we re-coded the raw values
364 of mean error (ANTerr), RT variability (ANTrtvar), and executive control efficiency (ANTcert),
365 multiplying them by -1 such that larger values would also imply better task performance. ANT
366 scores were obtained from sessions 1 and 3.

367 *Fluid intelligence.* Accuracy scores for the nine-item Raven's test (RavensAcc) were
368 computed for each participant, with higher scores implying better performance.

369

370 Table 2. Summary of behavioral metrics, including their task domain and a description of their
371 calculation. Raw values for ANTerr, ANTrtvar and ANTcert were re-coded such that larger
372 values indicated better task performance.

Task domain	Metric	Description
Attentional Blink	VABresid AABresid	Residuals from regressing out long-lag scores from short-lag scores.
Sustained Attention	VSARTdprime	Dprime scores.

	ASARTdprime	
	GradCPTdprime	
Selective Attention	ANTerr	Mean error across all trials.
	ANTrtvar	*SD*/*M* of correct-trial RTs.
	ANTaert	Alerting network efficiency. No-cue RT minus double-cue RT.
	ANToert	Orienting network efficiency. Center-cue RT minus spatial-cue RT.
	ANTcert	Executive control network efficiency. Incongruent RT minus congruent RT.
Fluid Intelligence	RavensAcc	Mean accuracy.

373

374

375 **MRI data collection and initial processing**

376 *Acquisition.* MRI data were acquired at the Clinical Imaging Research Centre (Singapore)
377 on a Siemens 3T MAGNETOM Prisma MRI scanner (Siemens, Erlangen, Germany) with a 32-
378 channel head coil. Scanning parameters were adapted from the Human Connectome Project
379 (HCP), and were chosen to ensure that full-brain coverage, including the cerebellum, was
380 achieved for each participant. MRI data were acquired in Sessions 1 and 5 of the study, with the
381 first session's data analyzed here. Each fMRI session started with a 5-min anatomical localizer
382 scan, followed by four 8-min resting-state scans, six 5.25-min task-based (VAB task) scans, and
383 a 5-min anatomical scan. During the resting-state runs, participants were asked to maintain
384 fixation at a cross displayed in the center of the screen.

385 *Imaging parameters.* A 3D high-resolution (1 mm x 1 mm x 1 mm) T1-weighted
386 MPRAGE pulse sequence was used to obtain whole-brain anatomical images for each
387 participant, allowing for subsequent normalization to standard space. For each participant, 128 1-

388 mm thick contiguous sagittal slices (0.5 mm skip; 1 x 1 mm in-plane resolution) were acquired.
389 Other scanning parameters included a repetition time (TR) of 2300 ms, an effective echo time
390 (TE) of 2.22 ms, a flip angle of 8^{o} and 260 mm field of view.
391 Functional MRI data were acquired with a multiband echoplanar imaging (MB-EPI;
392 CMRR release R2015; Feinberg et al., 2010; Moeller et al., 2010; Xu et al., 2013) sequence with
393 a MB acceleration factor of 8. 768 whole-brain images were obtained for each resting-state run
394 while 504 images were acquired for each task-based run. T2*-weighted images were acquired
395 using a TR of 625 ms, a TE of 33.2 ms and FA of 50^{o}. Interleaved slices (imaging matrix = 64 x
396 64) were collected using a 220 mm field of view, with slice thickness at 2.50 mm (no gap). The
397 effective voxel size was thus 2.5 x 2.5 x 2.5 mm^3.
398 *Preprocessing.* Both task and localizer data were pre-processed using a previously
399 published pipeline for functional connectivity analyses (Fong et al., 2019; Kong et al., 2019)
400 publicly available at
401 https://github.com/ThomasYeoLab/CBIG/tree/master/stable_projects/preprocessing/CBIG_fMRI
402 _Preproc2016. Pre-processing steps across resting-state and task-based runs were the same,
403 except when mentioned otherwise. First, the initial four frames from each run were removed to
404 aid with BOLD signal stabilisation. Motion correction using FSL's MCFLIRT was then applied
405 such that runs with more than 50% of the frames exceeding a motion threshold were discarded to
406 ameliorate any contributions of head motion. The motion threshold was defined as frame
407 displacement (FD) > 75 and frame-to-frame intensity (DVARS) > 0.2 (Power, Barnes, Snyder,
408 Schlaggar, & Petersen, 2012). From this step, one task-based run (and no resting-state runs) was
409 removed from our data. FSL's bbregister function was used for intrasubject registration of the T1
410 anatomical images to the T2*-weighted images. The best run for each subject was used as the

411 registration file across all functional runs. Subsequently, motion parameters and their derivatives,
412 the global whole brain signal, the white matter signal, the cerebral spinal fluid signal and linear
413 trends were regressed out. Additionally, for task-based runs, we regressed out the haemodynamic
414 response signal aligned to trial onset times. Frames with excessive motion, identified earlier on,
415 were interpolated over (Power et al., 2014), and a temporal filter was applied to retain
416 frequencies between 0.009 and 0.08 Hz. The resulting BOLD signal was projected to fsaverage6
417 surface space and spatially smoothed with an isotropic Gaussian kernel of 6 mm (FWHM).
418 *Functional connectivity.* Functional connectivity was evaluated in fsaverage6 surface
419 space for 400 cortical regions (Schaefer et al., 2017) and in MNI152 volumetric space for 19
420 subcortical regions (including the brain stem, and the left and right hemispheres of the
421 accumbens area, amygdala, caudate, cerebellum, ventral diencephalon, hippocampus, pallidum,
422 putamen, and thalamus), with a total of 419 parcellations. For each run, the mean time course of
423 all the parcellations were correlated using Pearson's product moment correlation, resulting in a
424 419 (rows) x 419 (columns) correlation matrix, with (419 x 419 – 419) / 2 = 87,571 unique
425 values. Each cell in the correlation matrix represents a functional connection (edge) between a
426 pair of parcellations. Fisher r-to-z transformation was applied to increase normality (Van Dijk et
427 al., 2010). For each participant, Fisher-transformed matrices for all four resting-state scans and
428 all six task-based scans were averaged separately, forming two functional connectivity (FC)
429 matrices: resting-state FC (RSFC) and Visual Attentional Blink task FC (VABFC).
430 *Motion control.* To reduce the effects of motion on functional connectivity, we adapted
431 motion control procedures from Rosenberg et al. (2018) to remove edges that were correlated
432 with motion. For each participant, we measured the following five motion parameters from their
433 resting-state and task-based scans: (i) maximum displacement, (ii) maximum rotation, (iii) mean

434 frame-to-frame displacement, (iv) mean frame displacement (FD), and (v) mean frame-to-frame
435 intensity (DVARS). Spearman's rank correlation was computed across participants between each
436 edge in the FC matrix and each motion parameter. To be comparable with Rosenberg et al.
437 (2018), in which 72.7% of edges remained after controlling for motion, we removed edges where
438 $r > .275$ (two-tailed $p < .02$), leaving 69,617 edges, or 79.50% of the initial 87,571 edges. Edges
439 were removed from both VABFC and RSFC if they met the criteria for removal in either FC
440 matrix.

441 **General approach for Connectome-based Predictive Models (CPM)**

442 We adapted the Connectome-based Predictive Model (CPM) approach (Finn et al., 2015;
443 Rosenberg, Finn, et al., 2016; Rosenberg et al., 2018; Shen et al., 2017) to predict individual
444 differences in behavior from functional connectivity information (Figure 2). In the following
445 section, we first describe our CPM procedure and then summarize our different models. Data
446 from all 73 participants were included in these analyses (71 for models involving the AAB score,
447 AABresid).
448

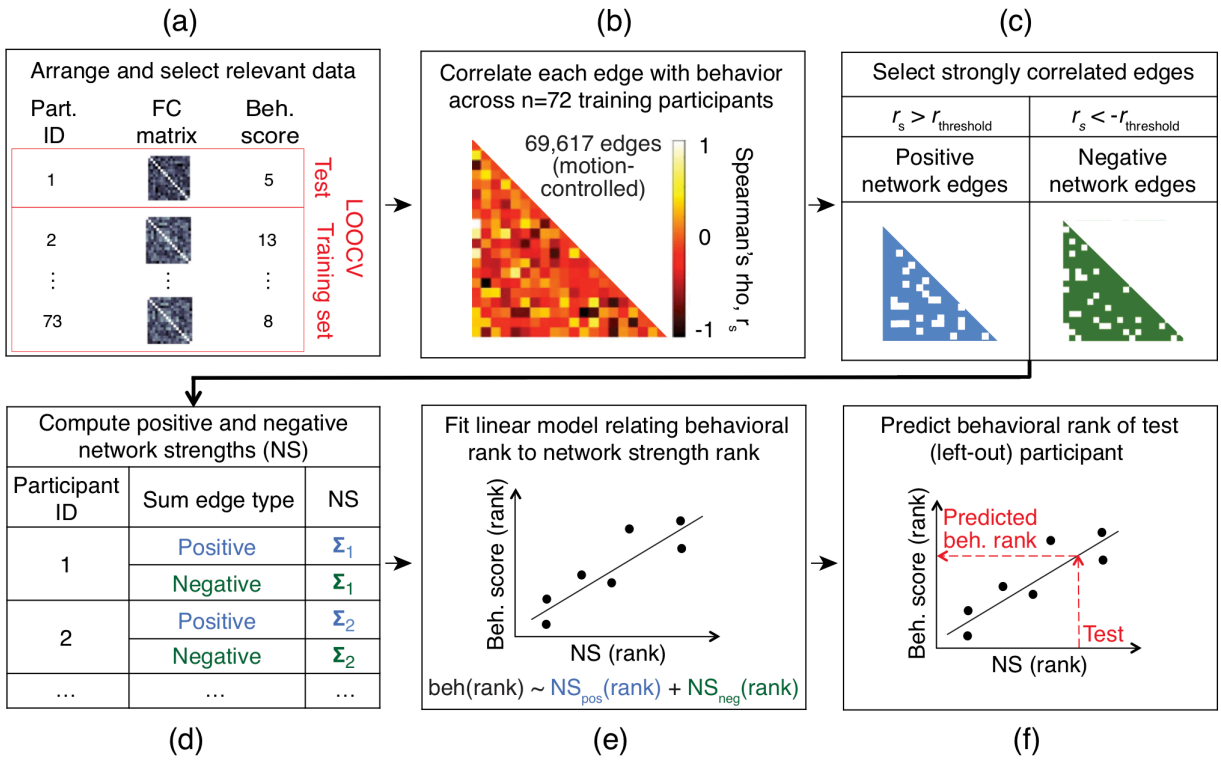

Figure 2. Procedure for Connectome-based Predictive Model (CPM) construction in the current study (adapted from Shen et al., 2017). CPMs predict individual differences in behavior from functional connectivity information. (a) Functional connectivity matrices and a behavioral score of interest for each participant were calculated. One pair was held out of model construction for each round of leave-one-out cross-validation (LOOCV) (Webb et al., 2011). (b) Functional connectivity edges were correlated with behavior across participants. (c) Edges that correlated most strongly, either positively or negatively, were selected. (d) Values from selected edges were summed separately for positive and negative network edges, yielding two network strengths for each participant. (e) A linear regression model relating (rank) network strengths to (rank) behavioral scores was computed. (f) The model was tested on a novel, out-of-sample participant (the individual left out in step (a)). After repeating steps a-f for each participant, the model was evaluated by correlating the predicted behavioral scores with the actual scores.

462

463 *Model training.* We first selected an FC matrix (i.e., VABFC or RSFC) and a behavioral
464 score (e.g., VABresid). As part of the leave-one-out cross-validation procedure (Figure 2a), we
465 then set aside the data for one participant as test data and proceeded to train the model on the
466 remaining data (n = 72). To identify edges that most strongly correlated with behavior, we
467 computed Spearman's rank correlations between each unique edge in the FC matrix and the
468 behavioral score across 72 participants (Figure 2b), yielding 69,617 Spearman's rho values (r_s).
469 Edges positively related to behavior (positive network edges) were identified as those whose r_s
470 was greater than a pre-defined threshold, $r_{threshold}$, and edges negatively related to behavior
471 (negative network edges) were defined as those whose r_s was less than $-r_{threshold}$ (Figure 2c).
472 Next, we computed network strengths (NS) for each participant by summing up values in their
473 individual FC matrices across all positively and negatively correlated edges (Figure 2d),
474 resulting in 72 sets of positive NS and negative NS values. Subsequently, we converted the
475 positive NS, negative NS, and behavioral scores to rank space by ordering them according to
476 participants' values. Finally, we formulated a multiple linear regression model (Figure 2e) with
477 positive NS rank and negative NS rank as independent variables and behavioral rank as the
478 dependent variable i.e., Behavior (rank) ~ $NS_{positive}$ (rank) + $NS_{negative}$ (rank).
479 *Model test.* We proceeded to predict the behavioral score (in rank space) of the test
480 participant (Figure 2f) by applying the training model to his/her FC matrix. Using the same
481 positive and negatively correlated edges identified from training, positive NS and negative NS
482 were first computed by summing up values in the FC matrix across the respective edges.
483 Following this step, positive and negative NS values of the test participant were ranked against

the relevant NS values of the training participants, and entered into the multiple linear regression model to predict a behavioral rank.

Model evaluation. As part of the leave-one-out cross-validation procedure, the above training and prediction steps were repeated on all participants ($N = 73$) such that each participant was left out of training once, resulting in 73 sets of predicted behavioral ranks. To measure the predictive power of the model, we obtained correlations between the predicted and observed values, controlling for motion (Rosenberg et al., 2018). To this end, partial Spearman's rank correlation was computed between predicted and observed behavioral ranks, with the motion parameters (see section on Motion control) included as covariates. Where FC matrices were different for training and test, motion parameters from both the resting-state and task-based scans were included (i.e., ten covariates); where the same FC matrix was used, only motion parameters from the relevant scan were included (i.e., five covariates). *P*-values for model evaluation were left uncorrected, as most of the comparisons represented planned replications of previous work, and the pattern of predictions across tasks was more informative than single model predictions. For other neuroimaging-based statistical tests, we corrected for multiple comparisons, as detailed in the respective Results sections (Functional connectivity and Network overlap).

CPM model specification for data from the current study

For each of the eleven behavioral scores (e.g., VABresid, AABresid, VSARTdprime, etc.), we repeated the CPM procedure to train and test four different types of models. Two model types (vabCPM model variants) were trained using FC information and behavioral responses acquired from the main VAB task (i.e., VABFC and VABresid), and used to predict behavioral performance of novel participants using either their VAB *task* (VABFC; Model type A), or their *rest* (RSFC; Model type B) FC information. With these models, we sought to identify attentional

networks that were predictive of good VAB performance (positive network) and poor VAB performance (negative network), and then to determine whether these networks generalized to make similar predictions about other tasks. Two other model types (task-specific model variants) were trained using task-specific behavioral data and either VAB *task* (VABFC; Model type C) or *rest* (RSFC; Model type D) information. Behavioral performance was then predicted from the same type of FC data that was used during training. With these models, we tested whether predictive networks for each task could be predicted from FC data that was unrelated to that task; any such predictive networks would be useful for identifying and comparing the edges that are predictive of performance on a given task.

Model type A (train on VABFC and behavioral data, predict with VABFC data). For training, the functional connectivity matrix VABFC and behavioral score VABresid were used to select edges and form the linear model. For test, the training model was applied to the VABFC matrix of the left-out participant. For evaluation, the predicted behavior from the leave-one-out procedure was correlated with the behavioral score from a selected task.

Model type B (train on VABFC and behavioral data, predict with RSFC data). As in the previous model, VABFC and VABresid were used for training, but for test, the training model was applied to the RSFC matrix of the left-out participant. For evaluation, the predicted behavior was correlated with the behavioral score from a selected task.

Model type C (train and test on VABFC data). During training, VABFC and the behavioral score from a selected task were used to form the model. During test, the training model was applied to VABFC of the left-out participant. For evaluation, the predicted behavior was correlated with the observed score of the selected task.

Model type D (train and test on RSFC data). For training, the functional connectivity matrix RSFC and the behavioral score from a selected task were used to form the model. For test, the training model was applied to the RSFC of the left-out participant. During evaluation, the predicted behavior was correlated with the observed score of the selected task.

Controls. For the primary analyses in the study, we implemented the CPM procedure using edge selection cutoffs ($r_{threshold}$ = .232, p = .05) previously used in Rosenberg et al. (2018). As an exploratory control, we also investigated whether our predictions were reasonably stable across edge selection cutoff values. To do so, we repeated the leave-one-out cross-validation procedure with $r_{threshold}$ ranging from .005 to .5, in steps of .005. Thus, in total, the CPM procedure was repeated (11 behavior x 4 models x 101 edge selection thresholds) 4,444 times.

As p-values from LOOCV procedures can be biased, we verified the significance of our models using permutation testing (Shen et al., 2017). A null distribution with 1000 iterations was generated for each $r_{threshold}$. For each iteration, we randomly shuffled participants' behavioral scores and repeated the prediction steps above. P-values (uncorrected for this exploratory analysis) were computed as the proportion of permutation r_s with values greater than the observed r_s.

Sustained Attention CPM from Rosenberg et al. (2016)

To compare our predictions and networks with another attention-related model, we applied the Sustained Attention CPM (saCPM) (Rosenberg, Finn, et al., 2016) to our FC data. The saCPM was constructed using FC data computed with 268 parcellations (Shen, Tokoglu, Papademetris, & Constable, 2013). As our FC data was computed with 419 parcellations (Schaefer et al., 2017), we transformed the Shen parcellations to Schaefer parcellations in MNI152 space (91x109x91, 2mm voxels). For each Shen parcellation, we located the

552 corresponding Schaefer parcellation at a corresponding spatial location, excluding those that
553 accounted for less than 10% of the voxels in the Shen parcellation. Next, we mapped the saCPM
554 edges in the following way: if Shen parcellation A mapped to Schaefer parcellations 1, 2, and 3
555 and Shen parcellation C mapped to Schaefer parcellations 7 and 8, a functional connection
556 (edge) between Shen parcellations A and C would be mapped to Schaefer edges 1-7, 2-7, 3-7, 1-
557 8, 2-8, and 3-8. As before, edges that were removed previously due to motion were also removed
558 in the mapped saCPM edges.

559 We computed network strengths by taking the dot product between the saCPM edges and
560 our FC matrix (VABFC or RSFC), and entered the result into a linear model: Behavior ~
561 $NS_{positive} + NS_{negative}$. Note that these were motion-controlled FCs (69,617 edges), but during
562 evaluation, we did not implement partial correlation with motion parameters as co-variates,
563 following Rosenberg, Finn, et al. (2016). As the saCPM model was trained using FC data and
564 dprime scores acquired during the GradCPT task, predicted scores from the model were also
565 dprime scores. We evaluated the result of applying the saCPM to our FC data by computing
566 Spearman's rank correlation between the predicted scores and the scores from each of our
567 behavioral tasks.

568 **Network overlaps and edge locations**

569 *Degree of overlap.* To better understand the relationships across CPMs, we calculated the
570 percentage of network overlap for model pairs. First, for each model, we identified edges that
571 were common across all iterations of the leave-one-out procedure; we reasoned that these edges
572 were most representative of the model. For each pair of models, we expressed the number of
573 edges in common percentages of the number of edges in each model, and we then computed the

574 average of the two percentages. These percentages were calculated separately for positive-
575 positive, negative-negative, positive-negative, and negative-positive network overlaps.
576 To statistically assess whether the edges for each pair of models significantly overlapped,
577 we used the hypergeometric cumulative density function to determine the probability of drawing
578 up to *x* out of *K* possible items with *n* drawings without replacement, from a population of size *M*
579 (Rosenberg, Zhang, et al., 2016). The procedure was implemented with the hygecdf function in
580 (*MATLAB*, 2014), as $p = 1 - \text{hygecdf}(x, M, K, n)$, with x as the number of overlapping edges, M
581 as the total number of edges, *K* as the number of edges from one model, and *n* as the number of
582 edges from the other model. To control for multiple comparisons, FDR correction was applied
583 across the complete set of tests (Benjamini & Hochberg, 1995).
584 *Anatomical location of networks and overlaps*. To determine the anatomical locations of
585 network edges and the overlaps between the vabCPM and saCPM networks, we first grouped the
586 419 parcellations into network groups. The parcellations were matched to 17 network labels
587 (Yeo et al., 2011), from which they were aggregated into eight cortical groups (Yeo, Tandi, &
588 Chee, 2015) and a subcortical group. For each pair of network groups (e.g. Visual and Salience /
589 Ventral Attention), we computed the number of connections (network edges) between them. We
590 then reported this value as a percentage of the total number of possible connections between that
591 pair of network groups.
592
593 **Results**
594 In the sections below, we first report the behavioral results and the functional
595 connectivity matrices. We then present the behavioral predictions based on models derived from
596 the present dataset, followed by the behavioral predictions based on an external model (the

saCPM; Rosenberg et al., 2016). After comparing the pattern of predictions, we compare the degree of overlap across the predictive networks. Finally, we examine the anatomical locations of the overlaps between the vabCPM and saCPM networks.

Behavioral performance

We found a robust visual attentional blink (VAB) in each session, with substantially impaired probe detection performance for the shorter lags (1, 2, 3) but not the longer lags (5, 7, 9) (Figure 3). For subsequent individual differences analyses, the VAB deficit was defined as short-lag performance when controlling for long-lag performance (see Methods), a definition the results supported. An AAB was also evidenced, though it was both smaller and less robust across sessions.

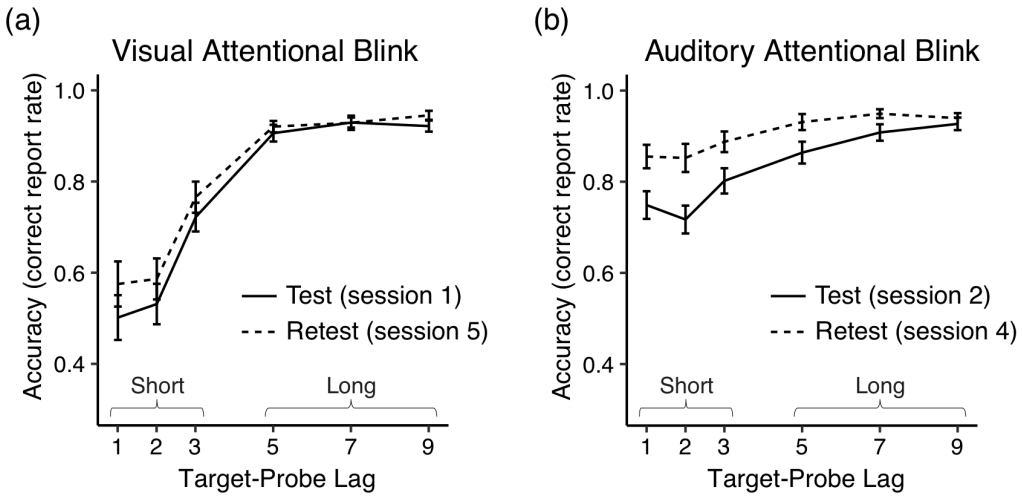

Figure 3. Accuracy scores (probe hit rates) for the VAB and AAB. Note the substantial impairment for the short target-probe lags (1, 2, and 3) in each session, especially for the VAB. Error bars represent standard error of the mean (SEM).

Test-retest reliability was high for most metrics, and their ranges were reasonable (

614 Table 3). Jarque-Bera tests of normality revealed that several behavioral scores were not
615 normally-distributed (see relevant plots in Figure 4). Hence we adopted non-parametric
616 approaches in our subsequent analyses and models.
617
618 Table 3. Summary of behavioral data. Test-retest reliability (Spearman correlations across
619 sessions) was high for most metrics and significant for all (ps < .002). Jarque-Bera tests indicated
620 some significant departures from normality. Metrics are presented before re-coding. Metrics that
621 were subsequently reversed so that larger values would indicate better task performance are
622 marked with an asterisk (*). $N = 73$ for all metrics except AABresid ($N = 71$).

Task domain	Metric	Mean	SD	Range	Reliability (r_s)	Jarque-Bera (p)
Attentional Blink	VABresid	0.003	0.213	[-0.577, 0.356]	0.75	.126
	AABresid	0.001	0.118	[-0.412, 0.274]	0.38	.002
Sustained Attention	VSARTdprime	3.469	0.77	[1.016, 5.256]	0.54	.077
	ASARTdprime	3.187	0.795	[0.364, 5.127]	0.62	.004
	GradCPTdprime	2.844	0.655	[1.607, 4.359]	0.65	.144
Selective Attention	*ANTerr (% incorrect)	2.463	2.222	[0, 11.111]	0.66	.001
	*ANTrtvar (s)	0.147	0.035	[0.088, 0.24]	0.65	.058
	ANTaert (s)	0.074	0.022	[0.02, 0.138]	0.42	.447
	ANToert (s)	0.04	0.017	[0, 0.085]	0.36	.500
	*ANTcert (s)	0.129	0.03	[0.078, 0.207]	0.74	.100
Fluid Intelligence	RavensAcc (% correct)	82.5	15.15	[22.22, 100]	-	.001

623

624 To examine how behavioral performance was related across the various tasks, we
625 computed Spearman's rank correlations between each pair of behavioral scores (Figure 4).
626 Significant correlations were primarily found within a given attentional domain. The three
627 measures of Sustained Attention (VSARTdprime, ASARTdprime and GradCPTdprime) were
628 significantly correlated, as were the primary measures of Selective Attention (ANTerr and
629 ANTrtvar) and some of their component measures. Many of these metrics were significantly
630 correlated, positively and negatively, across the Sustained and Selective Attention task domains
631 as well. The negative correlations with the alerting (ANTaert) and orienting (ANToert) metrics
632 may be due to their reflecting stimulus-driven attentional control, as opposed to the goal-directed
633 control required for many other metrics. Attentional Blink (VABresid and AABresid) and Fluid
634 Intelligence (RavensAcc) metrics generally were not significantly correlated with other metrics.
635

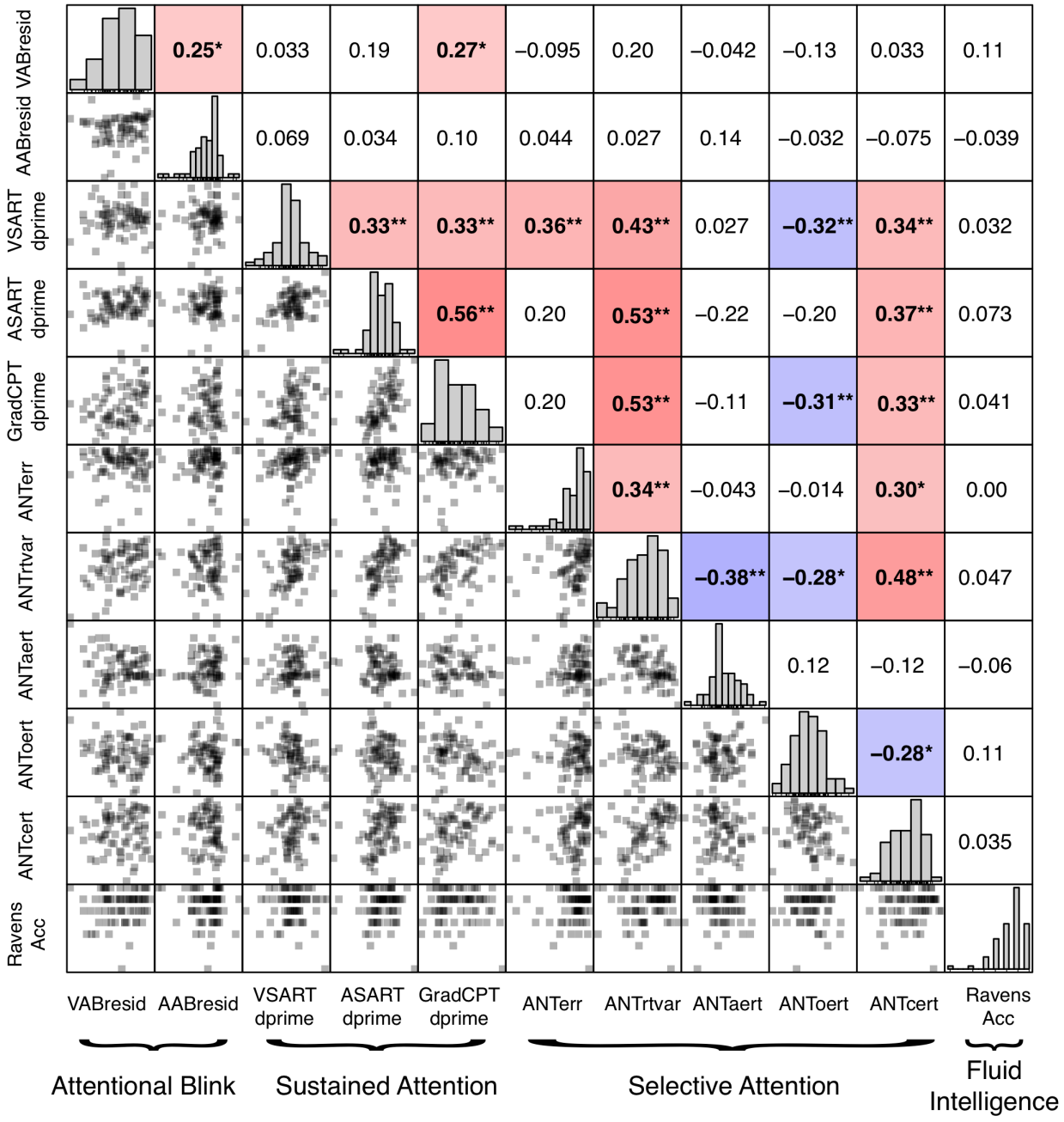

Figure 4. Behavioral score distributions and correlations. (Above diagonal) Spearman correlation coefficients for pairs of behavioral metrics. Most significant correlations were found within task domains, but some metrics correlated across the Sustained and Selective Attention domains. In contrast, Attentional Blink and Fluid Intelligence metrics largely did not correlate with other

641 metrics. Since the purpose of this analysis was to identify any behavioral relationships that might
642 explain subsequent CPM results, no correction for multiple comparisons was applied. *$p < .05$,
643 **$p < .01$. Red and blue shading indicates positive and negative relationships, respectively.
644 (Diagonal) Histograms of behavioral data. The behavioral data had been re-coded so that larger
645 values indicate better task performance for each measure. (Below diagonal) Scatterplots for each
646 pair of behavioral metrics.
647
648 **Functional connectivity matrices**
649 To assess and compare network connectivity during the VAB task and during rest, we
650 plotted group-averaged functional connectivity (FC) matrices (Figure 5). The 419 parcellations
651 from the FC matrices were matched to 17 network labels (Yeo et al., 2011), from which they
652 were aggregated into eight cortical groups (Yeo, Tandi, et al., 2015) and a subcortical group. FC
653 data from both the VAB task (VABFC; Figure 5a) and resting state (RSFC; Figure 5b) showed
654 similar connectivity patterns, with largely positive within-network correlations and mixed
655 directions for between-network correlations. The network correlation patterns were generally
656 similar to those observed in other data sets (Yeo et al., 2011; Yeo, Tandi, et al., 2015). Using
657 Network-based statistics to correct for multiple comparisons (Zalesky, Fornito, & Bullmore,
658 2010), we observed small differences between the two FC matrices, with many connections
659 linking the Salience/Ventral attention and the Dorsal attention networks (Figure 5c). Such
660 differences are consistent with the reported neural correlates of the attentional blink, which are in
661 frontal and parietal areas associated with the ventral and dorsal attention networks (Marois,
662 Chun, & Gore, 2000; Marois & Ivanoff, 2005).

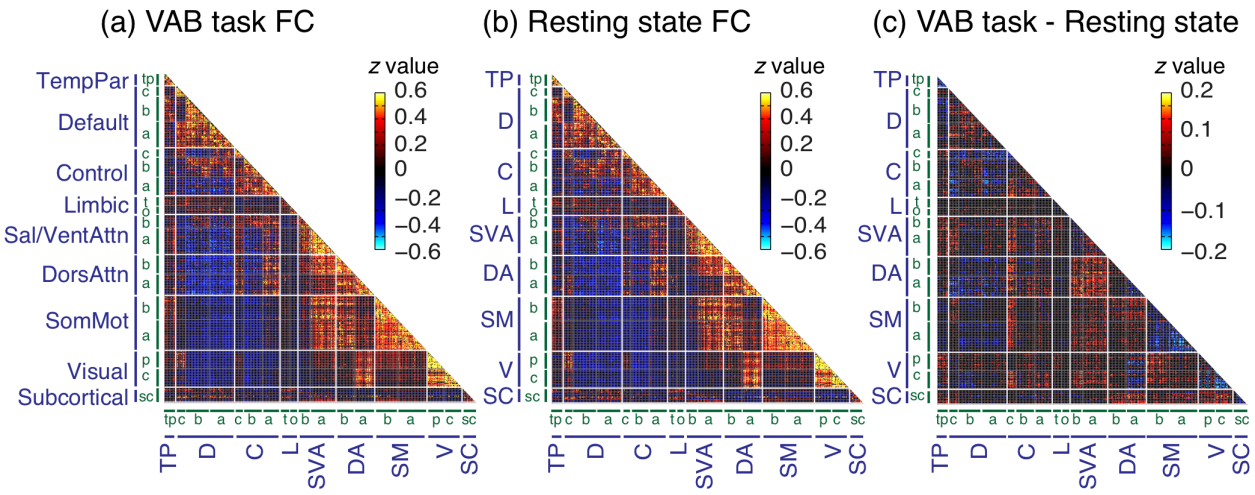

Figure 5. Functional connectivity (FC) matrices. Each edge was Fisher-transformed, and the resulting *z*-scores were averaged across participants. Edges found to correlate with motion were set to zero. (a) VAB task FC matrix (VABFC). (b) Resting-state FC matrix (RSFC). VABFC and RSFC patterns were similar to one another and to other data sets (Yeo et al., 2011; Yeo, Tandi, et al., 2015). (c) Difference FC matrix (VABFC - RSFC), showing edges that were significant at $p = .05$, corrected for multiple comparisons using network-based statistics. Differences between FC matrices were small, though they notably included connections linking the Salience/Ventral attention and the Dorsal attention networks. The 419 parcellations from the FC matrices were matched to 17 network labels (Yeo et al., 2011) (green labels), from which they were aggregated into eight cortical groups (Yeo, Tandi, et al., 2015) and a subcortical group (blue labels, spelled out in full in (a)). Subcortical regions include the brain stem, accumbens area, amygdala, caudate, cerebellum, ventral diencephalon, hippocampus, pallidum, putamen, and thalamus. For the green labels, letters represent the networks within the corresponding group, e.g., a(Default A), b(Default B), c(Default C), tp(TempPar), t(temporal pole in limbic region), o(orbital frontal cortex in limbic region), p(peripheral visual area), c(central visual area), and sc(subcortical).

680 **Behavioral predictions from CPMs constructed using the present dataset**

681 Models constructed from VAB functional connectivity and behavioral data (vabCPMs)
682 positively predicted VAB performance from task data (VABFC; Model type A) but not from
683 resting state data (RSFC; Model type B) (Figure 6a; corresponding values are tabulated in Figure
684 6-1 in the Extended Data). Task predictions were made in relative performance ranks (Spearman
685 correlations), so these predictions readily applied to other rank-order behavioral scores. When so
686 applied, we found that Fluid Intelligence performance could be positively predicted from both
687 task and rest FC data. Critically, the correlations between predicted and actual performance for
688 Sustained Attention metrics were *negative*, as were these correlations for Sustained Attention
689 tasks, albeit less consistently. Such results are counterintuitive, as all behavioral scores were re-
690 coded so that larger values indicated better performance. Furthermore, one might expect that
691 individuals whose network data predicted better performance on the VAB and Fluid Intelligence
692 tasks would perform worse on Sustained Attention and Selective Attention tasks. In reality,
693 however, VAB performance correlated insignificantly or weakly positively with other task
694 metrics, whereas Fluid Intelligence performance was not significantly correlated with any other
695 tasks. We return to this intriguing result in the Discussion.
696

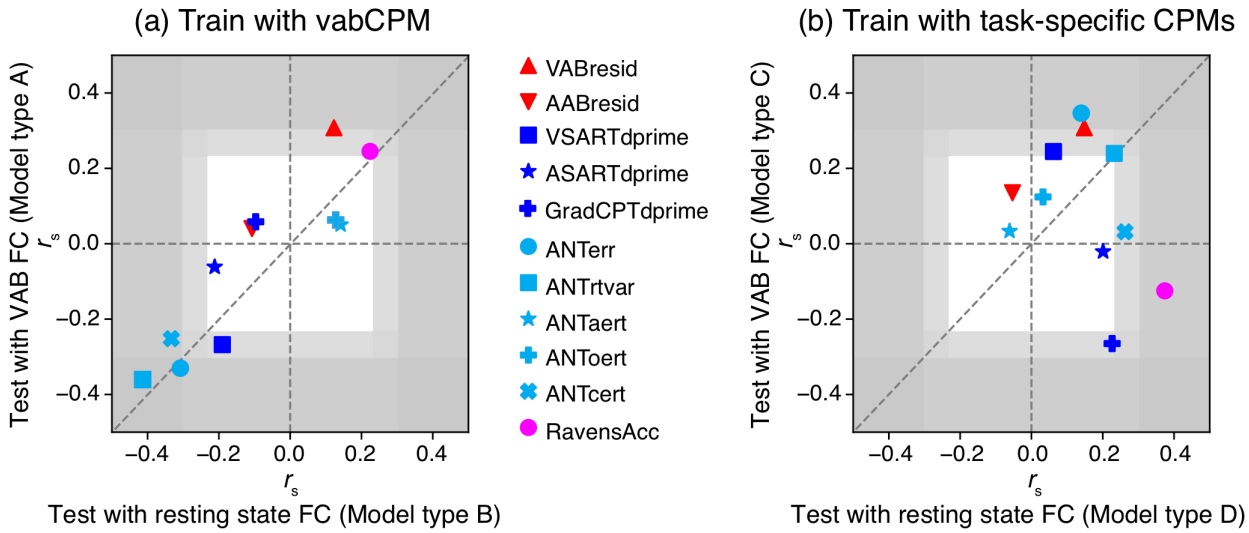

Figure 6. Behavioral predictions from CPMs. Each point represents a pair of Spearman's rank correlation coefficients (r_s) computed between observed and predicted behavioral scores for a given model type. (a) Predictions from vabCPMs, which were trained with VABFC and VABresid. Note the successful positive predictions for the VAB and Fluid Intelligence, but successful *negative* predictions for some Selective and Sustained Attention metrics. (b) Predictions from task-specific models. Many models could successfully predict behavioral performance, though results often varied greatly across the FC source. For both panels, the dark gray region indicates where r_s values are significant at the $p = .01$ level, and the lighter gray region indicates where r_s values are significant at the $p = .05$ level (uncorrected, with $d.f. = 71$). The r_s values and corresponding p-values are tabulated in Figure 6-1 in Extended Data. A standard edge selection threshold ($r_{threshold} = .232$, $p = .05$) was used for all models, though results were similar across a wide range of threshold values (Figure 6-2 and Figure 6-3 in Extended Data). Finally, as p-values from LOOCV procedures can be biased, we verified our results for the VAB using permutation testing; significance from this method and parametric approaches was consistent across edge selection thresholds (Figure 6-4 in in Extended Data).

Models built from task-specific behavioral data significantly predicted performance for each of the task metrics predicted from the vabCPMs, although the results were less consistent between VABFC-based (Model type C) and RSFC-based (Model type D) predictions (Figure 6b; corresponding values are tabulated in Figure 6-1 in the Extended Data). Although it is possible that the different predictions reflect different information in the two FC data sources (Figure 3), it is unclear whether the differences are stable or simply reflect difficulty in building models from fMRI data for which the behavioral data were collected separately. Indeed, CPMs constructed from fMRI data collected during task performance and that task's behavioral scores tend to be more robust (Rosenberg, Finn, et al., 2016; Rosenberg et al., 2018; Yoo et al., 2017). Regardless, due to the same FC-behavior pair being used during both training and test, significant negative predictions from the vabCPMs became positive, as expected (e.g., VSARTdprime, ANTerr, ANTrtvat and ANTcert).

To examine whether model predictions were sensitive to the number of edges selected during CPM training, we explored how r_s changes as a function of edge selection thresholds. R_s values were observed to be reasonably stable across edge selection thresholds, though more variation was observed in task-specific models (Model types C and D) than in vabCPMs (Model types A and B) (Figure 6-2 and Figure 6-3 in Extended Data). Additionally, as *p*-values from LOOCV procedures can be biased, we verified our results for the VAB using permutation testing; significance from this method and parametric approaches was consistent across edge selection thresholds (Figure 6-4 in in Extended Data). Each of these issues may have contributed to the unexpected negative predictions for the GradCPTdprime metric, an aspect of the results to which we return below.

Behavioral predictions from an external CPM (saCPM; Rosenberg et al., 2016).

For external validation of our model predictions, we applied the Sustained Attention CPM (saCPM) to our data. The saCPM was trained on fMRI and behavioral data from the GradCPT, a sustained attention task (Rosenberg, Finn, et al., 2016). When applied to our data, the saCPM predictions were virtually mirror images of our vabCPM predictions (Figure 7). Specifically, whereas the vabCPM predicted VAB and Fluid Intelligence performance positively and predicted Sustained Attention and Selective Attention performance negatively, the saCPM predicted VAB and Fluid Intelligence performance *negatively* and predicted Sustained Attention and Selective Attention performance *positively*.

With these findings, we also replicated the results from Rosenberg et al. (2018). Specifically, the saCPM was able to predict the error rates (ANTerr), reaction time variability (ANTrtvar), and conflict (ANTcert) metrics for novel individuals in the ANT task. Conversely, we failed to replicate the significant predictions for GradCPTdprime in our data, contrary to expectations. This replication failure is puzzling because the GradCPT behavioral data showed a reasonable spread of scores and good test-retest reliability (Table 3), and the saCPM and vabCPM did make significant predictions on other Sustained Attention metrics in our data set. We are currently exploring our GradCPT task and results further in our laboratory.

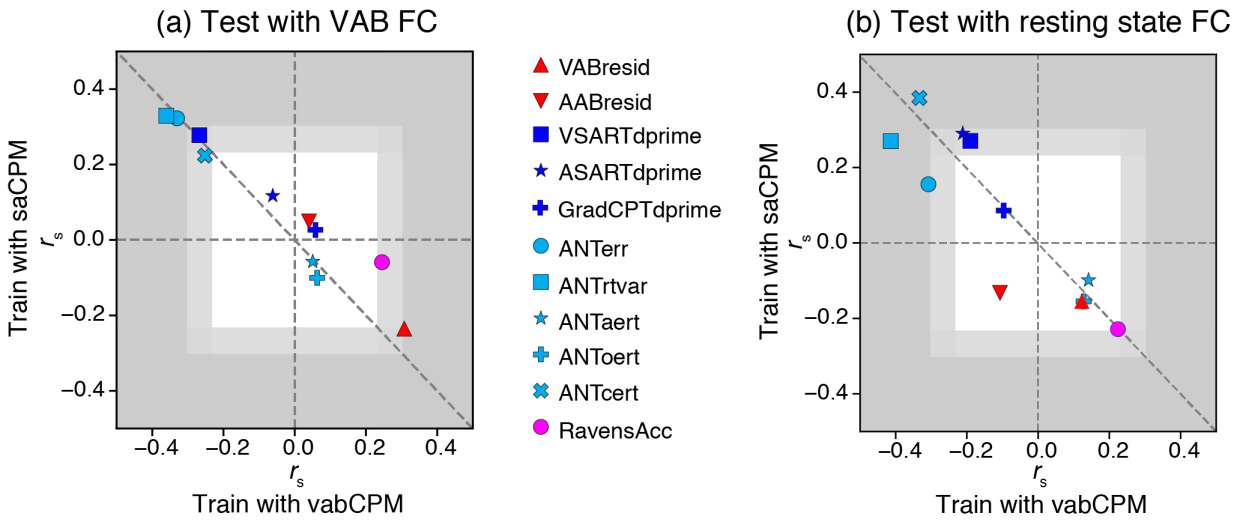

Figure 7. Comparison of predictions from the vabCPM and saCPM. Each point represents a pair of Spearman's rank correlation coefficients (r_s) computed between observed and predicted behavioral scores for a given model type. (a) Predictions from VABFC data. Note the saCPM's successful positive predictions for some Selective and Sustained Attention metrics, with a successful *negative* prediction for the VAB. As noted above, the prediction directions were reversed for the vabCPM; indeed, the prediction points fall close to the diagonal. (b) Predictions from RSFC data. The vabCPM and saCPM predictions went in opposite directions, and were generally similar to the predictions from the VABFC. For both panels, the dark gray region indicates where r_s values are significant at the $p = .01$ level, and the lighter gray region indicates where r_s values are significant at the $p = .05$ level (uncorrected, with $d.f. = 71$). The edge selection threshold ($r_{threshold}$) corresponded to $p = .05$ for all models. The r_s values and corresponding p-values for the saCPM are tabulated in Figure 7-1 in the Extended Data. (See Figure 6 for additional vabCPM details.)

Degree of overlap between predictive network pairs

To better understand how the underlying functional connectivity networks contributed to the model predictions, we analyzed the extent to which edges were shared between pairs of CPMs. For each pair, we calculated overlaps between positive network edges (those that predicted better behavioral performance for the model's task), between negative network edges, and across positive and negative network edges (Figure 8). The networks derived from the vabCPM (VAB network) and saCPM (SA network) did not significantly overlap at similar network edges (e.g. positive-positive; Figure 8a and 8b). Instead, they significantly overlapped only at *opposing* network edges, the positive edges from one model and the negative edges from the other (Figure 8c and 8d).

The overlaps between the VAB network and SA network accorded with their overlaps with networks derived from other task-specific CPMs. VAB network edges tended to overlap more with the opposing network edges of the Sustained and Selective Attention models (Figure 8c and 8d) as compared to their similar network edges (Figure 8a and 8b). In contrast, SA network edges overlapped significantly with similar edges from each of the Sustained and Selective Attention models, but with none of their opposing edges. Finally, although VAB and Fluid Intelligence networks overlapped significantly only at similar network edges, SA network edges did not significantly overlap with either similar or opposing Fluid Intelligence network edges.

Taken together, the pattern of edge overlaps accords with the pattern of behavioral predictions. The VAB and SA networks overlapped at opposing edges, and their predictions were also negatively related (Figure 7). Predictions for individual metrics also aligned with model overlaps. In general, when a metric's observed scores positively correlated with scores

predicted from the vabCPM or saCPM, that metric's CPM-derived network tended to overlap with the VAB or SA network at similar network edges.

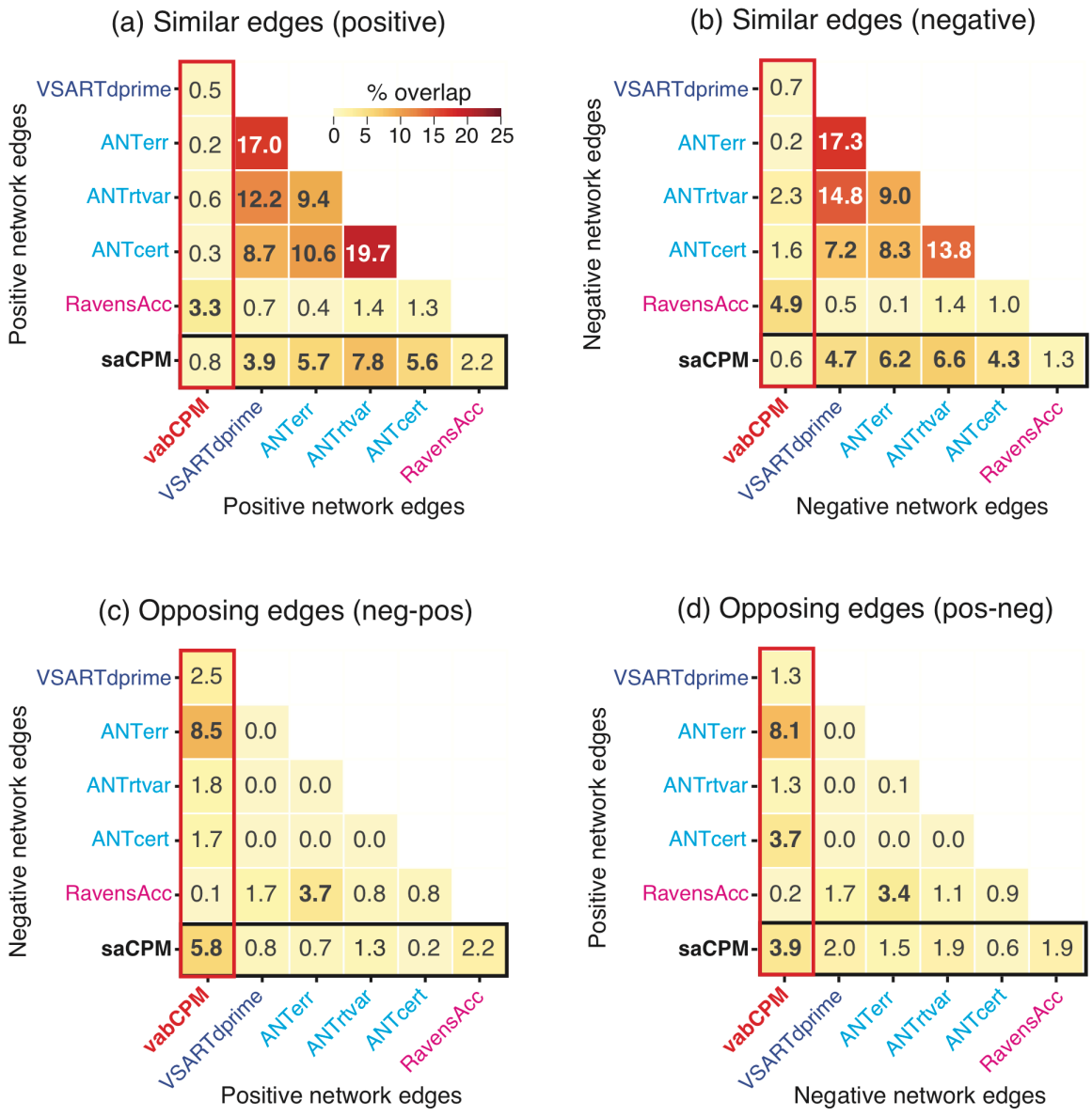

Figure 8. Percentage of edge overlap between networks from selected pairs of CPMs. Each task-specific model was based on VABFC data (Model type C). Model pairs with statistically significant overlap ($p < .05$, FDR corrected) are indicated in bold. Positive network edges predicted better behavioral performance for their associated metric, whereas negative network

edges predicted worse behavioral performance. Overlap between *similar* network edges, (a) positive-positive and (b) negative-negative. Sustained Attention (including the saCPM) and Selective Attention models overlap primarily on similar edges, as do Fluid Intelligence and the vabCPM. Overlap between *opposing* network edges, (c) negative-positive and (d) positive-negative. The vabCPM network primarily overlaps with Sustained Attention (including the saCPM) and Selective Attention on their opposing edges. Only task metrics that were significantly predicted by vabCPMs using VABFC information are shown. The full set of overlaps for all CPMs can be found in the Extended Data (Figure 8-1, 8-2, 8-3, and 8-4). Note that the highest overlap value for any pairwise comparison, including each task metric predicted from VABFC and RSFC, was 26.5%.

We also observed significant overlaps between similar network edges from Sustained and Selective Attention models (Figure 8a and 8b). Similarly, Rosenberg and colleagues observed substantial overlaps between a high attention (positive) network from the GradCPT task and networks predicting high accuracy and low RT variability (better performance) in the ANT (Rosenberg et al., 2018). Taken together, these results suggest that sustained and selective attention share similar functional networks, at least in part. Such results also justify labels such as the "successful attention network" (Rosenberg et al., 2018). Importantly, these network overlaps are consistent with both the CPM predictions and the behavioral relationships (Figure 4). Significant network overlaps involving the VAB network, however, were not accompanied by significant behavioral relationships. We return to this observation in the Discussion.

Anatomical locations of network edges

To better understand the networks that contribute to the successful behavioral predictions from the vabCPM and the saCPM, we investigated the anatomy of their underlying network edges. Briefly, for each pair of network groups (e.g. Visual and Salience / Ventral Attention), we expressed the number of shared connections (network edges) as a percentage of the number of possible connections between that pair (Figure 9). Edges that positively predicted VAB performance occurred primarily between the Default network and several other networks, including the Salience/Ventral attention, Dorsal attention, and Somatomotor networks (Figure 9a). For negative network edges, the most frequent connections occurred between the Salience/Ventral attention network and several other networks, including the Dorsal attention, Somatomotor, and Visual networks (Figure 9b). Note that such connections were also enhanced in VABFC compared to RSFC (Figure 5c), and that the connections across attention networks are consistent with the neural correlates of the attentional blink (Marois et al., 2000; Marois & Ivanoff, 2005). Negative network edges were also frequently found in Somatomotor network connections to the Dorsal attention network and to itself (within-network connections).

The SA network's positive edges primarily included connections that involved the Visual and Subcortical network groups (Figure 9d). This pattern represents the remapping of the connections between the cerebellum and the occipital lobe of the "high attention" network (Rosenberg, Finn, et al., 2016) from the Shen-268 parcellation (Shen et al., 2013) to the Schaefer-419 one (Schaefer et al., 2017). Negative network edges included within-group connections in the TempPar and Subcortical networks (Figure 9c), which accord well with the intra-temporal, intra-cerebellar, and temporo-parietal connections in the "low attention" network (Rosenberg, Finn, et al., 2016). We observed additional negative edges within the Visual network and from the TempPar network to various other networks.

(a) VAB, positive network edge locations

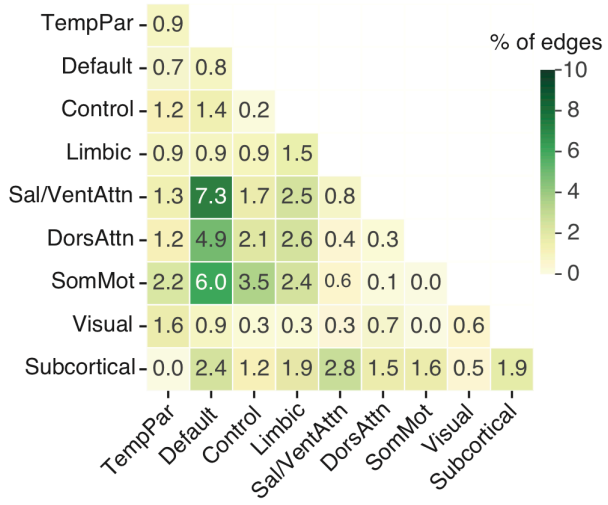

(b) VAB, negative network edge locations

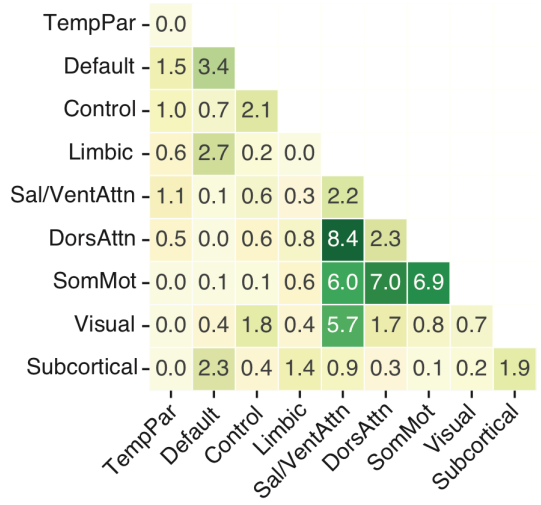

(c) SA, negative network edge locations

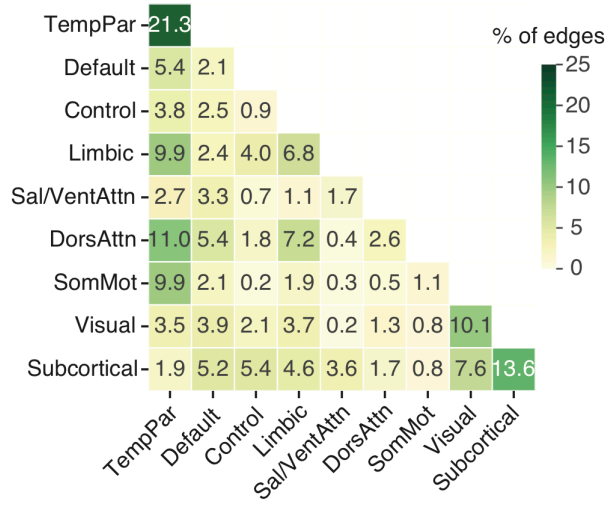

(d) SA, positive network edge locations

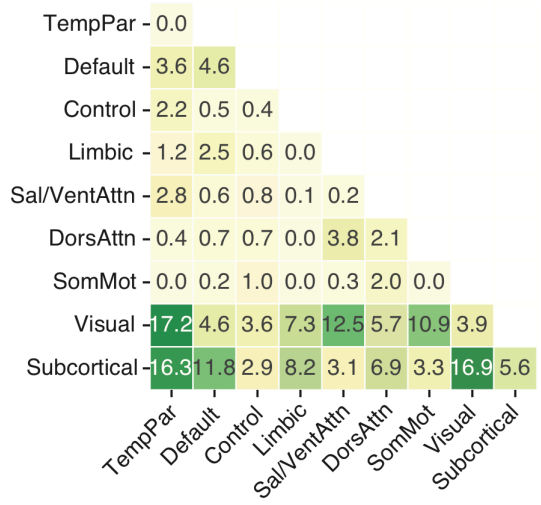

(e) Edge overlap; positive VAB, negative SA

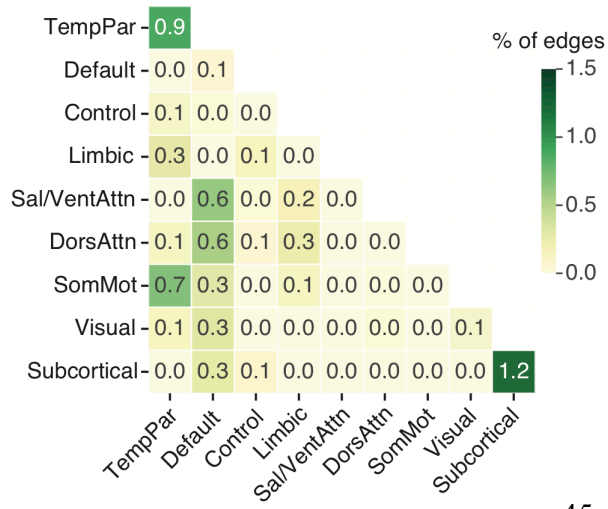

(f) Edge overlap; negative VAB, positive SA

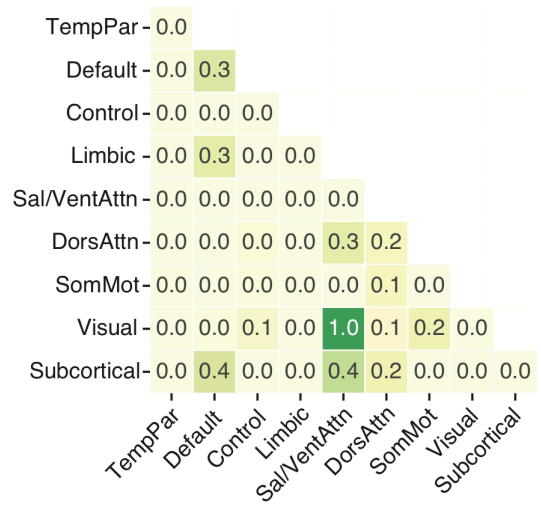

Figure 9. Anatomical locations of predictive attentional network edges. Each cell represents the number of shared connections between a pair of network groups, expressed as a percentage of the number of possible connections between that pair. For details about network groups, see Figure 5. (a) Positive and (b) negative VAB network edges. (c) Negative and (d) positive SA network edges. The panel order has been reversed for easier comparison with the opposing edges from the VAB network. (e) Positive VAB network edges and negative SA network edges (i.e. overlaps between (a) and (c)). (f) Negative VAB network edges and positive SA network edges (i.e. overlaps between (b) and (d)). Overlap percentages were numerically small, but included key network groups, particularly Default and Salience / Ventral Attention (Sal/VentAttn).

Although the VAB and SA networks involved largely dissociable sets of edges, some critical edges appeared to be shared (Figure 9e and 9f). Note that these overlaps were at opposing edges (Figure 8). Although overlap percentages were numerically small, they included key network groups. In particular, multiple identified connections involved the Default, Salience/Ventral attention, or TempPar networks.

Discussion

Predictive attentional networks

We used Connectome-based Predictive Modeling (CPM), a machine learning-based technique that associates task performance with functional connectivity measures, to construct a predictive model of Visual Attentional Blink (VAB) performance. Our model (vabCPM) successfully predicted VAB performance in novel individuals from fMRI data. The model's predictions generalized to other task domains, including fluid intelligence (Finn et al., 2015).

869 Critically, vabCPM predictions for many sustained and selective attention task scores correlated
870 *negatively* with the actual scores. As such, these significant predictions represent both model
871 generalization and an extension of previous CPM results (Rosenberg, Finn, et al., 2016;
872 Rosenberg et al., 2018; Yoo et al., 2017), but with new insights into attentional function owing to
873 the divergent predictions.

874 For external validation of these results, we applied the Sustained Attention CPM
875 (saCPM) (Rosenberg, Finn, et al., 2016), to our data. Previously, the saCPM successfully
876 predicted task performance for sustained attention (GradCPT) (Rosenberg, Finn, et al., 2016) and
877 selective attention (Attention Network Task, ANT) (Rosenberg et al., 2018). Here we broadly
878 replicated these results: The saCPM successfully predicted sustained and selective attention task
879 performance when applied to our participants' data. In the sustained attention domain, however,
880 significant predictions were found only for visual and auditory SART (Sustained Attention to
881 Response Task) scores, but curiously not for GradCPT scores. In results that mirrored the
882 vabCPM predictions, the saCPM predictions for VAB scores were negatively correlated with the
883 observed scores.

884 This pattern of divergent predictions was also reflected in network overlaps. For the
885 networks derived from the vabCPM and the saCPM, *opposing* network edges (i.e. positive from
886 one, negative from the other) overlapped significantly, whereas similar network edges did not.
887 Models constructed from each behavioral task and our fMRI data corroborated these results. As
888 all behavioral data had been coded such that larger values indicated better performance, these
889 divergent predictions indicate that "good" or "bad" network function was contingent on the task
890 and its cognitive underpinnings. Moreover, the tasks were performed over several days,

suggesting that the individual differences were stable and trait-like, not due to session-specific state effects.

Implications for Cognitive Mechanisms

Although the observed pattern of CPM predictions may seem counterintuitive, it is consistent with both empirical evidence and theoretical positions. Foremost, our study's attention tasks represent different ways of deploying voluntary attention. The VAB task requires rapid attentional engagement, disengagement, and re-engagement; sustained attention tasks require engagement over a prolonged period of time; the attention network task (ANT) requires the direction of attention to relevant spatial information. Skogsberg et al. (2015) proposed that the VAB and sustained attention tasks lie at opposite ends of a transient-sustained attention continuum. Rensink suggested that the VAB and ANT involve different core attentional functions: In the VAB, 'attentional holding' of one visual object leads to the failure to create a second visual object, whereas in the ANT, 'attentional filtering' selects spatial information (Rensink, 2013, 2015).

Empirical findings support the relative uniqueness of the VAB, while also suggesting that the ANT and sustained attention are more closely related. In our data, we found a general lack of behavioral correlations between the VAB and other attention task measures, consistent with previous studies of individual differences (Dale et al., 2013; Skogsberg et al., 2015). Conversely, we found moderately strong correlations between sustained attention tasks and the ANT. These tasks have been found to share similar functional networks (Rosenberg et al., 2018), a result we also replicated.

Nevertheless, the conceptual separation of the VAB from other attention tasks does not explain the *opposing* pattern of predictions from the same networks (saCPM and vabCPM), and

914 the significant overlaps between their opposing network edges. Two observations provide
915 important context for this finding. First, the VAB has spawned a variety of theoretical accounts
916 (Dux & Marois, 2009), and its magnitude is sensitive to numerous disparate manipulations,
917 ranging from requiring online responses (Jolicoeur, 1998) to concurrently listening to music
918 (Olivers & Nieuwenhuis, 2005). As such, the VAB may have multiple causes. Second, our VAB
919 predictions were generally moderate (r = .31 for vabCPM and r = .24 for saCPM; 5-10% of the
920 variance), far smaller than the observed degree of stable individual differences (test-retest: r =
921 .71; 50% of the variance). It is possible that the CPMs capture the variance associated with few,
922 or even one, of the factors that affect VAB magnitude. If so, what could that factor be?
923 One plausible explanation is that our predictions reflect an individual's propensity to
924 maintain a more diffuse state of attention. This idea is consistent with the overinvestment
925 hypothesis, in which the VAB results from too much attention being allocated to the first target;
926 consequently, reducing attention on the RSVP stream improves performance (Dale & Arnell,
927 2010, 2015; Olivers & Nieuwenhuis, 2006). Similarly, task-concurrent mind-wandering, such as
928 listening to music or thinking about a vacation, reduces the VAB deficit (Olivers &
929 Nieuwenhuis, 2005, 2006). Similar effects are found in studies of disposition: Individuals with a
930 greater propensity for mind-wandering tend to perform better in the VAB task (Thomson et al.,
931 2015). Furthermore, mind-wandering has been linked to higher fluid intelligence and better
932 problem-solving abilities (Baird, Smallwood, & Schooler, 2011; Godwin et al., 2017; Unsworth
933 & McMillan, 2014), consistent with our CPM findings.
934 Diffuse attentional states, however, are associated with lower performance on tasks
935 requiring more focused cognition. For example, in sustained attention tasks, individuals more
936 prone to lapses in attention perform more poorly on the SART (Manly, 1999; Robertson et al.,

1997; Smilek et al., 2010). Within individuals, distractive thoughts are associated with lower SART accuracy, prolonged and more variable RTs, and poorer response inhibition (Kam & Handy, 2014; Leszczynski et al., 2017; Stawarczyk, Majerus, Maj, Van der Linden, & D'Argembeau, 2011). In selective attention tasks, individuals more prone to mind-wandering performed worse on the ANT task (Gonçalves et al., 2017), and showed impaired exogeneous orienting of attention (Hu et al., 2012).

Both mind-wandering states and traits are also reflected in patterns of brain activity. Activity in the Default network and frontoparietal control regions increases during mind-wandering (Fox, Spreng, Ellamil, Andrews-Hanna, & Christoff, 2015). Similarly, individuals more prone to mind-wander had increased connectivity both within the Default network and between the Default network and frontoparietal control regions (Godwin et al., 2017). Such results are partially consistent with our findings. Edges between the Default and attentional networks (not the Control network) were related to positive VAB network edges and negative SA network edges.

On the weight of the available evidence, we propose that our vabCPM reflects individuals' propensity towards diffuse attentional deployment. That propensity could indicate an individual's ability to diffusely attend, their tendency to be in that state or mode, or both. We also suggest that other CPMs, including the saCPM, could reflect the complementary propensity towards more focused attentional deployment.

Predictions from "Resting State"

Neuroimaging studies using 'resting state' data, in which subjects are scanned while not engaged in any particular task, have become increasingly popular. Initially used to identify functional architecture (Biswal, Yetkin, Haughton, & Hyde, 1995; Schaefer et al., 2017; Yeo et

al., 2011), resting state data have recently been used to test whether functional architecture persists even when an individual is not engaged in a task that requires a given neurocognitive network (Finn et al., 2015; Jangraw et al., 2018; Lin et al., 2018; Rosenberg, Finn, et al., 2016; Yoo et al., 2017). Resting state studies also have many logistical advantages, including relatively easy standardization across multiple test sites and the potential for numerous applications from a single data set. In the current study, resting state CPMs (Model type D) replicated previous studies by successfully predicting sustained attention (Yoo et al., 2017), selective attention (Yoo et al., 2017) and fluid intelligence (Finn et al., 2015) task performance. We also replicated the result that models trained with *task-concurrent* FC data generally predict task performance better than models trained from resting state data (Yoo et al., 2017). Finally, when applying our trained vabCPM model to novel participants, predictions from task FC data were superior to predictions from resting-state FC data (Finn et al., 2017; Greene, Gao, Scheinost, & Constable, 2018; Rosenberg, Finn, et al., 2016; Rosenberg et al., 2018). This result might be due to amplification of behaviorally relevant individual differences in network patterns while performing a task (Greene et al., 2018).

Methodological Considerations

Although we followed the guidelines in Shen et al. (2017) when developing our CPMs, there are two notable methodological differences. First, previous studies used the volumetric Shen-268 parcellation (Shen et al., 2013), but we used the surface-based Schaefer-419 parcellation (Schaefer et al., 2017). Second, previous studies have constructed linear models for associating network strength and behavioral scores, with predictions assessed using Spearman correlations (Fountain-Zaragoza et al., 2019; Lin et al., 2018; Rosenberg, Finn, et al., 2016; Rosenberg et al., 2018). We instead formed linear models from the ranks directly. Despite these

983 differences, we still observed prediction patterns that were largely consistent and comparable to

984 previous studies, providing evidence that CPMs are reasonably robust across such variations.

985

References

Adolfsdottir, S., Sorensen, L., & Lundervold, A. J. (2008). The attention network test: A characteristic pattern of deficits in children with ADHD. *Behavioral and Brain Functions*, *4*(1), 9. https://doi.org/10.1186/1744-9081-4-9

Asplund, C. L., Todd, J. J., Snyder, A. P., & Marois, R. (2010). A central role for the lateral prefrontal cortex in goal-directed and stimulus-driven attention. *Nature Neuroscience*, *13*(4), 507–512. https://doi.org/10.1038/nn.2509

Baird, B., Smallwood, J., & Schooler, J. W. (2011). Back to the future: Autobiographical planning and the functionality of mind-wandering. *Consciousness and Cognition*, *20*(4), 1604–1611. https://doi.org/10.1016/j.concog.2011.08.007

Benjamini, Y., & Hochberg, Y. (1995). Controlling the False Discovery Rate: A Practical and Powerful Approach to Multiple Testing. *Journal of the Royal Statistical Society. Series B (Methodological)*, *57*(1), 289–300.

Bilker, W. B., Hansen, J. A., Brensinger, C. M., Richard, J., Gur, R. E., & Gur, R. C. (2012). Development of Abbreviated Nine-Item Forms of the Raven's Standard Progressive Matrices Test. *Assessment*, *19*(3), 354–369. https://doi.org/10.1177/1073191112446655

Biswal, B., Yetkin, F. Z., Haughton, V. M., & Hyde, J. S. (1995). Functional connectivity in the motor cortex of resting human brain using echo-planar MRI. *Magnetic Resonance in Medicine*, *34*(4), 537–541.

Chun, M. M., Golomb, J. D., & Turk-Browne, N. B. (2011). A Taxonomy of External and Internal Attention. *Annual Review of Psychology*, *62*(1), 73–101. https://doi.org/10.1146/annurev.psych.093008.100427

1008 Chun, M. M., & Potter, M. C. (1995). A two-stage model for multiple target detection in rapid
1009 serial visual presentation. *Journal of Experimental Psychology. Human Perception and*
1010 *Performance*, *21*(1), 109–127.
1011 Corbetta, M., & Shulman, G. L. (2002). Control of goal-directed and stimulus-driven attention in
1012 the brain. *Nature Reviews Neuroscience*, *3*(3), 201–215. https://doi.org/10.1038/nrn755
1013 Dale, G., & Arnell, K. M. (2010). Individual differences in dispositional focus of attention
1014 predict attentional blink magnitude. *Attention, Perception, & Psychophysics*, *72*(3), 602–
1015 606. https://doi.org/10.3758/APP.72.3.602
1016 Dale, G., & Arnell, K. M. (2015). Multiple measures of dispositional global/local bias predict
1017 attentional blink magnitude. *Psychological Research*, *79*(4), 534–547.
1018 https://doi.org/10.1007/s00426-014-0591-3
1019 Dale, G., Dux, P. E., & Arnell, K. M. (2013). Individual differences within and across attentional
1020 blink tasks revisited. *Attention, Perception, & Psychophysics*, *75*(3), 456–467.
1021 https://doi.org/10.3758/s13414-012-0415-8
1022 Desimone, R., & Duncan, J. (1995). Neural Mechanisms of Selective Visual Attention. *Annual*
1023 *Review of Neuroscience*, *18*(1), 193–222.
1024 https://doi.org/10.1146/annurev.ne.18.030195.001205
1025 Di Lollo, V., Kawahara, J., Shahab Ghorashi, S. M., & Enns, J. T. (2005). The attentional blink:
1026 Resource depletion or temporary loss of control? *Psychological Research*, *69*(3), 191–
1027 200. https://doi.org/10.1007/s00426-004-0173-x
1028 Duncan, J. (2010). The multiple-demand (MD) system of the primate brain: Mental programs for
1029 intelligent behaviour. *Trends in Cognitive Sciences*, *14*(4), 172–179.
1030 https://doi.org/10.1016/j.tics.2010.01.004

1031 Dux, P. E., & Marois, R. (2009). The attentional blink: A review of data and theory. *Attention,*
1032 *Perception & Psychophysics*, *71*(8), 1683–1700. https://doi.org/10.3758/APP.71.8.1683
1033 Egeth, H. E., & Yantis, S. (1997). Visual attention: Control, representation, and time course.
1034 *Annual Review of Psychology*, *48*(1), 269–297.
1035 Esterman, M., Noonan, S. K., Rosenberg, M., & DeGutis, J. (2013). In the Zone or Zoning Out?
1036 Tracking Behavioral and Neural Fluctuations During Sustained Attention. *Cerebral*
1037 *Cortex*, *23*(11), 2712–2723. https://doi.org/10.1093/cercor/bhs261
1038 Fan, J., McCandliss, B. D., Sommer, T., Raz, A., & Posner, M. I. (2002). Testing the Efficiency
1039 and Independence of Attentional Networks. *Journal of Cognitive Neuroscience*, *14*(3),
1040 340–347. https://doi.org/10.1162/089892902317361886
1041 Feinberg, D. A., Moeller, S., Smith, S. M., Auerbach, E., Ramanna, S., Glasser, M. F., …
1042 Yacoub, E. (2010). Multiplexed Echo Planar Imaging for Sub-Second Whole Brain
1043 FMRI and Fast Diffusion Imaging. *PLoS ONE*, *5*(12), e15710.
1044 https://doi.org/10.1371/journal.pone.0015710
1045 Finn, E. S., Scheinost, D., Finn, D. M., Shen, X., Papademetris, X., & Constable, R. T. (2017).
1046 Can brain state be manipulated to emphasize individual differences in functional
1047 connectivity? *NeuroImage*, *160*, 140–151.
1048 https://doi.org/10.1016/j.neuroimage.2017.03.064
1049 Finn, E. S., Shen, X., Scheinost, D., Rosenberg, M. D., Huang, J., Chun, M. M., … Constable, R.
1050 T. (2015). Functional connectome fingerprinting: Identifying individuals using patterns
1051 of brain connectivity. *Nature Neuroscience*, *18*(11), 1664–1671.
1052 https://doi.org/10.1038/nn.4135

1053 Fong, A. H. C., Yoo, K., Rosenberg, M. D., Zhang, S., Li, C.-S. R., Scheinost, D., … Chun, M.
1054 M. (2019). Dynamic functional connectivity during task performance and rest predicts
1055 individual differences in attention across studies. *NeuroImage*, *188*, 14–25.
1056 https://doi.org/10.1016/j.neuroimage.2018.11.057
1057 Fountain-Zaragoza, S., Samimy, S., Rosenberg, M. D., & Prakash, R. S. (2019). Connectome-
1058 based models predict attentional control in aging adults. *NeuroImage*, *186*, 1–13.
1059 https://doi.org/10.1016/j.neuroimage.2018.10.074
1060 Fox, K. C. R., Spreng, R. N., Ellamil, M., Andrews-Hanna, J. R., & Christoff, K. (2015). The
1061 wandering brain: Meta-analysis of functional neuroimaging studies of mind-wandering
1062 and related spontaneous thought processes. *NeuroImage*, *111*, 611–621.
1063 https://doi.org/10.1016/j.neuroimage.2015.02.039
1064 Godwin, C. A., Hunter, M. A., Bezdek, M. A., Lieberman, G., Elkin-Frankston, S., Romero, V.
1065 L., … Schumacher, E. H. (2017). Functional connectivity within and between intrinsic
1066 brain networks correlates with trait mind wandering. *Neuropsychologia*, *103*, 140–153.
1067 https://doi.org/10.1016/j.neuropsychologia.2017.07.006
1068 Gonçalves, Ó. F., Rêgo, G., Oliveira-Silva, P., Leite, J., Carvalho, S., Fregni, F., … Boggio, P. S.
1069 (2017). Mind wandering and the attention network system. *Acta Psychologica*, *172*, 49–
1070 54. https://doi.org/10.1016/j.actpsy.2016.11.008
1071 Greene, A. S., Gao, S., Scheinost, D., & Constable, R. T. (2018). Task-induced brain state
1072 manipulation improves prediction of individual traits. *Nature Communications*, *9*(1).
1073 https://doi.org/10.1038/s41467-018-04920-3

1074 Hu, N., He, S., & Xu, B. (2012). Different efficiencies of attentional orienting in different
1075 wandering minds. *Consciousness and Cognition*, *21*(1), 139–148.
1076 https://doi.org/10.1016/j.concog.2011.12.007
1077 Jangraw, D. C., Gonzalez-Castillo, J., Handwerker, D. A., Ghane, M., Rosenberg, M. D.,
1078 Panwar, P., & Bandettini, P. A. (2018). A functional connectivity-based neuromarker of
1079 sustained attention generalizes to predict recall in a reading task. *NeuroImage*, *166*, 99–
1080 109. https://doi.org/10.1016/j.neuroimage.2017.10.019
1081 Jolicoeur, P. (1998). Modulation of the attentional blink by on-line response selection: Evidence
1082 from speeded and unspeeded Task1 decisions. *Memory & Cognition*, *26*(5), 1014–1032.
1083 https://doi.org/10.3758/BF03201180
1084 Kam, J. W. Y., & Handy, T. C. (2014). Differential recruitment of executive resources during
1085 mind wandering. *Consciousness and Cognition*, *26*, 51–63.
1086 https://doi.org/10.1016/j.concog.2014.03.002
1087 Kong, R., Li, J., Orban, C., Sabuncu, M. R., Liu, H., Schaefer, A., … Yeo, B. T. T. (2019).
1088 Spatial Topography of Individual-Specific Cortical Networks Predicts Human Cognition,
1089 Personality, and Emotion. *Cerebral Cortex*, *29*(6), 2533–2551.
1090 https://doi.org/10.1093/cercor/bhy123
1091 Leszczynski, M., Chaieb, L., Reber, T. P., Derner, M., Axmacher, N., & Fell, J. (2017). Mind
1092 wandering simultaneously prolongs reactions and promotes creative incubation. *Scientific*
1093 *Reports*, *7*(1). https://doi.org/10.1038/s41598-017-10616-3
1094 Lin, Q., Rosenberg, M. D., Yoo, K., Hsu, T. W., O'Connell, T. P., & Chun, M. M. (2018).
1095 Resting-State Functional Connectivity Predicts Cognitive Impairment Related to

1096 Alzheimer's Disease. *Frontiers in Aging Neuroscience*, *10*.
1097 https://doi.org/10.3389/fnagi.2018.00094
1098 Lundervold, A. J., Adolfsdottir, S., Halleland, H., Halmøy, A., Plessen, K., & Haavik, J. (2011).
1099 Attention Network Test in adults with ADHD - the impact of affective fluctuations.
1100 *Behavioral and Brain Functions*, *7*(1), 27. https://doi.org/10.1186/1744-9081-7-27
1101 MacLean, M. H., & Arnell, K. M. (2012). A conceptual and methodological framework for
1102 measuring and modulating the attentional blink. *Attention, Perception, & Psychophysics*,
1103 *74*(6), 1080–1097. https://doi.org/10.3758/s13414-012-0338-4
1104 Manly, T. (1999). The absent mind: Further investigations of sustained attention to response.
1105 *Neuropsychologia*, *37*(6), 661–670. https://doi.org/10.1016/S0028-3932(98)00127-4
1106 Marois, R., Chun, M. M., & Gore, J. C. (2000). Neural correlates of the attentional blink.
1107 *Neuron*, *28*(1), 299–308.
1108 Marois, R., & Ivanoff, J. (2005). Capacity limits of information processing in the brain. *Trends*
1109 *in Cognitive Sciences*, *9*(6), 296–305. https://doi.org/10.1016/j.tics.2005.04.010
1110 *MATLAB*. (2014). Natick, MA: The MathWorks, Inc.
1111 Moeller, S., Yacoub, E., Olman, C. A., Auerbach, E., Strupp, J., Harel, N., & Uğurbil, K. (2010).
1112 Multiband multislice GE-EPI at 7 tesla, with 16-fold acceleration using partial parallel
1113 imaging with application to high spatial and temporal whole-brain fMRI. *Magnetic*
1114 *Resonance in Medicine*, *63*(5), 1144–1153. https://doi.org/10.1002/mrm.22361
1115 Olivers, C. N. L., & Nieuwenhuis, S. (2005). The Beneficial Effect of Concurrent Task-
1116 Irrelevant Mental Activity on Temporal Attention. *Psychological Science*, *16*(4), 265–
1117 269. https://doi.org/10.1111/j.0956-7976.2005.01526.x

1118 Olivers, C. N. L., & Nieuwenhuis, S. (2006). The beneficial effects of additional task load,
1119 positive affect, and instruction on the attentional blink. *Journal of Experimental*
1120 *Psychology: Human Perception and Performance*, *32*(2), 364–379.
1121 https://doi.org/10.1037/0096-1523.32.2.364
1122 Peirce, J. W. (2007). PsychoPy—Psychophysics software in Python. *Journal of Neuroscience*
1123 *Methods*, *162*(1–2), 8–13. https://doi.org/10.1016/j.jneumeth.2006.11.017
1124 Posner, M. I., & Petersen, S. E. (1990). The Attention System of the Human Brain. *Annual*
1125 *Review of Neuroscience*, *13*(1), 25–42.
1126 https://doi.org/10.1146/annurev.ne.13.030190.000325
1127 Power, J. D., Barnes, K. A., Snyder, A. Z., Schlaggar, B. L., & Petersen, S. E. (2012). Spurious
1128 but systematic correlations in functional connectivity MRI networks arise from subject
1129 motion. *NeuroImage*, *59*(3), 2142–2154.
1130 https://doi.org/10.1016/j.neuroimage.2011.10.018
1131 Power, J. D., Mitra, A., Laumann, T. O., Snyder, A. Z., Schlaggar, B. L., & Petersen, S. E.
1132 (2014). Methods to detect, characterize, and remove motion artifact in resting state fMRI.
1133 *NeuroImage*, *84*, 320–341. https://doi.org/10.1016/j.neuroimage.2013.08.048
1134 Raven, J., Raven, J. C., & Court, J. H. (1998). *Manual for Raven's progressive matrices and*
1135 *vocabulary scales*. Oxford: Oxford Psychologists.
1136 Raymond, J. E., Shapiro, K. L., & Arnell, K. M. (1992). Temporary suppression of visual
1137 processing in an RSVP task: An attentional blink? *Journal of Experimental Psychology.*
1138 *Human Perception and Performance*, *18*(3), 849–860.
1139 Rensink, R. A. (2013). Perception and Attention. In D. Reisberg (Ed.), *Oxford Handbook of*
1140 *Cognitive Psychology* (pp. 97–116). New York: Oxford University Press.

Rensink, R. A. (2015). A Function-Centered Taxonomy of Visual Attention. In P. Coates & S. Coleman (Eds.), *Phenomenal Qualities: Sense, Perception, and Consciousness*. (pp. 347–375). Oxford: Oxford University Press.

Robertson, I. H., Manly, T., Andrade, J., Baddeley, B. T., & Yiend, J. (1997). `Oops!': Performance correlates of everyday attentional failures in traumatic brain injured and normal subjects. *Neuropsychologia*, *35*(6), 747–758. https://doi.org/10.1016/S0028-3932(97)00015-8

Rosenberg, M. D., Finn, E. S., Scheinost, D., Papademetris, X., Shen, X., Constable, R. T., & Chun, M. M. (2016). A neuromarker of sustained attention from whole-brain functional connectivity. *Nature Neuroscience*, *19*(1), 165–171. https://doi.org/10.1038/nn.4179

Rosenberg, M. D., Hsu, W.-T., Scheinost, D., Constable, T. R., & Chun, M. M. (2018). Connectome-based Models Predict Separable Components of Attention in Novel Individuals. *Journal of Cognitive Neuroscience*, *30*(2), 160–173. https://doi.org/10.1162/jocn_a_01197

Rosenberg, M. D., Noonan, S., DeGutis, J., & Esterman, M. (2013). Sustaining visual attention in the face of distraction: A novel gradual-onset continuous performance task. *Attention, Perception, & Psychophysics*, *75*(3), 426–439. https://doi.org/10.3758/s13414-012-0413-x

Rosenberg, M. D., Zhang, S., Hsu, W.-T., Scheinost, D., Finn, E. S., Shen, X., … Chun, M. M. (2016). Methylphenidate Modulates Functional Network Connectivity to Enhance Attention. *Journal of Neuroscience*, *36*(37), 9547–9557. https://doi.org/10.1523/JNEUROSCI.1746-16.2016

1163 Schaefer, A., Kong, R., Gordon, E. M., Laumann, T. O., Zuo, X.-N., Holmes, A. J., … Yeo, B.
1164 T. T. (2017). Local-Global Parcellation of the Human Cerebral Cortex from Intrinsic
1165 Functional Connectivity MRI. *Cerebral Cortex*, 1–20.
1166 https://doi.org/10.1093/cercor/bhx179
1167 Seli, P., Cheyne, J. A., Barton, K. R., & Smilek, D. (2012). Consistency of sustained attention
1168 across modalities: Comparing visual and auditory versions of the SART. *Canadian*
1169 *Journal of Experimental Psychology/Revue Canadienne de Psychologie Expérimentale*,
1170 *66*(1), 44–50. https://doi.org/10.1037/a0025111
1171 Shen, X., Finn, E. S., Scheinost, D., Rosenberg, M. D., Chun, M. M., Papademetris, X., &
1172 Constable, R. T. (2017). Using connectome-based predictive modeling to predict
1173 individual behavior from brain connectivity. *Nature Protocols*, *12*(3), 506–518.
1174 https://doi.org/10.1038/nprot.2016.178
1175 Shen, X., Tokoglu, F., Papademetris, X., & Constable, R. T. (2013). Groupwise whole-brain
1176 parcellation from resting-state fMRI data for network node identification. *NeuroImage*,
1177 *82*, 403–415. https://doi.org/10.1016/j.neuroimage.2013.05.081
1178 Skogsberg, K., Grabowecky, M., Wilt, J., Revelle, W., Iordanescu, L., & Suzuki, S. (2015). A
1179 relational structure of voluntary visual-attention abilities. *Journal of Experimental*
1180 *Psychology: Human Perception and Performance*, *41*(3), 761–789.
1181 https://doi.org/10.1037/a0039000
1182 Smilek, D., Carriere, J. S. A., & Cheyne, J. A. (2010). Failures of sustained attention in life, lab,
1183 and brain: Ecological validity of the SART. *Neuropsychologia*, *48*(9), 2564–2570.
1184 https://doi.org/10.1016/j.neuropsychologia.2010.05.002

1185 Stawarczyk, D., Majerus, S., Maj, M., Van der Linden, M., & D'Argembeau, A. (2011). Mind-
1186 wandering: Phenomenology and function as assessed with a novel experience sampling
1187 method. *Acta Psychologica*, *136*(3), 370–381.
1188 https://doi.org/10.1016/j.actpsy.2011.01.002
1189 Tamber-Rosenau, B. J., Dux, P. E., Tombu, M. N., Asplund, C. L., & Marois, R. (2013). Amodal
1190 Processing in Human Prefrontal Cortex. *Journal of Neuroscience*, *33*(28), 11573–11587.
1191 https://doi.org/10.1523/JNEUROSCI.4601-12.2013
1192 Thomson, D. R., Ralph, B. C. W., Besner, D., & Smilek, D. (2015). The more your mind
1193 wanders, the smaller your attentional blink: An individual differences study. *Quarterly*
1194 *Journal of Experimental Psychology*, *68*(1), 181–191.
1195 https://doi.org/10.1080/17470218.2014.940985
1196 Unsworth, N., & McMillan, B. D. (2014). Similarities and differences between mind-wandering
1197 and external distraction: A latent variable analysis of lapses of attention and their relation
1198 to cognitive abilities. *Acta Psychologica*, *150*, 14–25.
1199 https://doi.org/10.1016/j.actpsy.2014.04.001
1200 Van Dijk, K. R. A., Hedden, T., Venkataraman, A., Evans, K. C., Lazar, S. W., & Buckner, R. L.
1201 (2010). Intrinsic functional connectivity as a tool for human connectomics: Theory,
1202 properties, and optimization. *Journal of Neurophysiology*, *103*(1), 297–321.
1203 https://doi.org/10.1152/jn.00783.2009
1204 Webb, G. I., Sammut, C., Perlich, C., Horváth, T., Wrobel, S., Korb, K. B., … Raedt, L. D.
1205 (2011). Leave-One-Out Cross-Validation. In C. Sammut & G. I. Webb (Eds.),
1206 *Encyclopedia of Machine Learning* (pp. 600–601). https://doi.org/10.1007/978-0-387-
1207 30164-8_469

1208 Wojtowicz, M., Berrigan, L. I., & Fisk, J. D. (2012). Intra-individual Variability as a Measure of
1209 Information Processing Difficulties in Multiple Sclerosis. *International Journal of MS*
1210 *Care*, *14*(2), 77–83. https://doi.org/10.7224/1537-2073-14.2.77
1211 Xu, J., Moeller, S., Auerbach, E. J., Strupp, J., Smith, S. M., Feinberg, D. A., … Uğurbil, K.
1212 (2013). Evaluation of slice accelerations using multiband echo planar imaging at 3T.
1213 *NeuroImage*, *83*, 991–1001. https://doi.org/10.1016/j.neuroimage.2013.07.055
1214 Yeo, B. T. T., Krienen, F. M., Eickhoff, S. B., Yaakub, S. N., Fox, P. T., Buckner, R. L., …
1215 Chee, M. W. L. (2015). Functional Specialization and Flexibility in Human Association
1216 Cortex. *Cerebral Cortex*, *25*(10), 3654–3672. https://doi.org/10.1093/cercor/bhu217
1217 Yeo, B. T. T., Krienen, F. M., Sepulcre, J., Sabuncu, M. R., Lashkari, D., Hollinshead, M., …
1218 Buckner, R. L. (2011). The organization of the human cerebral cortex estimated by
1219 intrinsic functional connectivity. *Journal of Neurophysiology*, *106*(3), 1125–1165.
1220 https://doi.org/10.1152/jn.00338.2011
1221 Yeo, B. T. T., Tandi, J., & Chee, M. W. L. (2015). Functional connectivity during rested
1222 wakefulness predicts vulnerability to sleep deprivation. *NeuroImage*, *111*, 147–158.
1223 https://doi.org/10.1016/j.neuroimage.2015.02.018
1224 Yoo, K., Rosenberg, M. D., Hsu, W.-T., Zhang, S., Li, C.-S. R., Scheinost, D., … Chun, M. M.
1225 (2017). Connectome-based predictive modeling of attention: Comparing different
1226 functional connectivity features and prediction methods across datasets. *NeuroImage*.
1227 https://doi.org/10.1016/j.neuroimage.2017.11.010
1228 Zalesky, A., Fornito, A., & Bullmore, E. T. (2010). Network-based statistic: Identifying
1229 differences in brain networks. *NeuroImage*, *53*(4), 1197–1207.
1230 https://doi.org/10.1016/j.neuroimage.2010.06.041

Legends

Table 1. Schedule of tasks and data used in analysis. Participants were encouraged to take breaks between the tasks to prevent fatigue. With the exception of the Raven's Progressive Matrices test, each task was performed twice on non-successive days. Task domains and tasks were as follows. Attentional Blink: Visual Attentional Blink (VAB) and Auditory Attentional Blink (AAB). Sustained Attention: Visual Sustained Attention to Response Task (VSART), Auditory Sustained Attention to Response Task (ASART), and Gradual-onset Continuous Performance Task (GradCPT). Selective Attention: Attentional Network Task (ANT). Fluid Intelligence: Raven's Progressive Matrices test (Raven's).

Figure 1. Experimental paradigm for the visual attentional blink (VAB) task. Participants identified a target and then detected a probe within a stream of distractors, responding when prompted at the conclusion of the stream. The target was a red letter, the probe was a white letter X, and distractors were other white letters. The auditory attentional blink (AAB) task was similar, save targets were complex tones, the probe was a high-pitched pure tone, and distractors were other pure tones. SOA = stimulus onset asynchrony.

Table 2. Summary of behavioral metrics, including their task domain and a description of their calculation. Raw values for ANTerr, ANTrtvar and ANTcert were re-coded such that larger values indicated better task performance.

Figure 2. Procedure for Connectome-based Predictive Model (CPM) construction in the current study (adapted from Shen et al., 2017). CPMs predict individual differences in behavior from

functional connectivity information. (a) Functional connectivity matrices and a behavioral score of interest for each participant were calculated. One pair was held out of model construction for each round of leave-one-out cross-validation (LOOCV) (Webb et al., 2011). (b) Functional connectivity edges were correlated with behavior across participants. (c) Edges that correlated most strongly, either positively or negatively, were selected. (d) Values from selected edges were summed separately for positive and negative network edges, yielding two network strengths for each participant. (e) A linear regression model relating (rank) network strengths to (rank) behavioral scores was computed. (f) The model was tested on a novel, out-of-sample participant (the individual left out in step (a)). After repeating steps a-f for each participant, the model was evaluated by correlating the predicted behavioral scores with the actual scores.

Figure 3. Accuracy scores (probe hit rates) for the VAB and AAB. Note the substantial impairment for the short target-probe lags (1, 2, and 3) in each session, especially for the VAB. Error bars represent standard error of the mean (SEM).

Table 3. Summary of behavioral data. Test-retest reliability (Spearman correlations across sessions) was high for most metrics and significant for all (*p*s < .002). Jarque-Bera tests indicated some significant departures from normality. Metrics are presented before re-coding. Metrics that were subsequently reversed so that larger values would indicate better task performance are marked with an asterisk (*). N = 73 for all metrics except AABresid (N = 71).

Figure 4. Behavioral score distributions and correlations. (Above diagonal) Spearman correlation coefficients for pairs of behavioral metrics. Most significant correlations were found within task

domains, but some metrics correlated across the Sustained and Selective Attention domains. In contrast, Attentional Blink and Fluid Intelligence metrics largely did not correlate with other metrics. Since the purpose of this analysis was to identify any behavioral relationships that might explain subsequent CPM results, no correction for multiple comparisons was applied. *$p < .05$, **$p < .01$. Red and blue shading indicates positive and negative relationships, respectively. (Diagonal) Histograms of behavioral data. The behavioral data had been re-coded so that larger values indicate better task performance for each measure. (Below diagonal) Scatterplots for each pair of behavioral metrics.

Figure 5. Functional connectivity (FC) matrices. Each edge was Fisher-transformed, and the resulting *z*-scores were averaged across participants. Edges found to correlate with motion were set to zero. (a) VAB task FC matrix (VABFC). (b) Resting-state FC matrix (RSFC). VABFC and RSFC patterns were similar to one another and to other data sets (Yeo et al., 2011; Yeo, Tandi, et al., 2015). (c) Difference FC matrix (VABFC - RSFC), showing edges that were significant at $p = .05$, corrected for multiple comparisons using network-based statistics. Differences between FC matrices were small, though they notably included connections linking the Salience/Ventral attention and the Dorsal attention networks. The 419 parcellations from the FC matrices were matched to 17 network labels (Yeo et al., 2011) (green labels), from which they were aggregated into eight cortical groups (Yeo, Tandi, et al., 2015) and a subcortical group (blue labels, spelled out in full in (a)). Subcortical regions include the brain stem, accumbens area, amygdala, caudate, cerebellum, ventral diencephalon, hippocampus, pallidum, putamen, and thalamus. For the green labels, letters represent the networks within the corresponding group, e.g., a(Default

A), b(Default B), c(Default C), tp(TempPar), t(temporal pole in limbic region), o(orbital frontal cortex in limbic region), p(peripheral visual area), c(central visual area), and sc(subcortical).

Figure 6. Behavioral predictions from CPMs. Each point represents a pair of Spearman's rank correlation coefficients (r_s) computed between observed and predicted behavioral scores for a given model type. (a) Predictions from vabCPMs, which were trained with VABFC and VABresid. Note the successful positive predictions for the VAB and Fluid Intelligence, but successful *negative* predictions for some Selective and Sustained Attention metrics. (b) Predictions from task-specific models. Many models could successfully predict behavioral performance, though results often varied greatly across the FC source. For both panels, the dark gray region indicates where r_s values are significant at the $p = .01$ level, and the lighter gray region indicates where r_s values are significant at the $p = .05$ level (uncorrected, with $d.f. = 71$). The r_s values and corresponding p-values are tabulated in Figure 6-1 in Extended Data. A standard edge selection threshold ($r_{threshold} = .232$, $p = .05$) was used for all models, though results were similar across a wide range of threshold values (Figure 6-2 and Figure 6-3 in Extended Data). Finally, as p-values from LOOCV procedures can be biased, we verified our results for the VAB using permutation testing; significance from this method and parametric approaches was consistent across edge selection thresholds (Figure 6-4 in in Extended Data).

Figure 7. Comparison of predictions from the vabCPM and saCPM. Each point represents a pair of Spearman's rank correlation coefficients (r_s) computed between observed and predicted behavioral scores for a given model type. (a) Predictions from VABFC data. Note the saCPM's successful positive predictions for some Selective and Sustained Attention metrics, with a

successful *negative* prediction for the VAB. As noted above, the prediction directions were reversed for the vabCPM; indeed, the prediction points fall close to the diagonal. (b) Predictions from RSFC data. The vabCPM and saCPM predictions went in opposite directions, and were generally similar to the predictions from the VABFC. For both panels, the dark gray region indicates where r_s values are significant at the $p = .01$ level, and the lighter gray region indicates where r_s values are significant at the $p = .05$ level (uncorrected, with $d.f. = 71$). The edge selection threshold ($r_{threshold}$) corresponded to $p = .05$ for all models. The r_s values and corresponding p-values for the saCPM are tabulated in Figure 7-1 in the Extended Data. (See Figure 6 for additional vabCPM details.)

Figure 8. Percentage of edge overlap between networks from selected pairs of CPMs. Each task-specific model was based on VABFC data (Model type C). Model pairs with statistically significant overlap ($p < .05$, FDR corrected) are indicated in bold. Positive network edges predicted better behavioral performance for their associated metric, whereas negative network edges predicted worse behavioral performance. Overlap between *similar* network edges, (a) positive-positive and (b) negative-negative. Sustained Attention (including the saCPM) and Selective Attention models overlap primarily on similar edges, as do Fluid Intelligence and the vabCPM. Overlap between *opposing* network edges, (c) negative-positive and (d) positive-negative. The vabCPM network primarily overlaps with Sustained Attention (including the saCPM) and Selective Attention on their opposing edges. Only task metrics that were significantly predicted by vabCPMs using VABFC information are shown. The full set of overlaps for all CPMs can be found in the Extended Data (Figure 8-1, 8-2, 8-3, and 8-4). Note

that the highest overlap value for any pairwise comparison, including each task metric predicted from VABFC and RSFC, was 26.5%.

Figure 9. Anatomical locations of predictive attentional network edges. Each cell represents the number of shared connections between a pair of network groups, expressed as a percentage of the number of possible connections between that pair. For details about network groups, see Figure 5. (a) Positive and (b) negative VAB network edges. (c) Negative and (d) positive SA network edges. The panel order has been reversed for easier comparison with the opposing edges from the VAB network. (e) Positive VAB network edges and negative SA network edges (i.e. overlaps between (a) and (c)). (f) Negative VAB network edges and positive SA network edges (i.e. overlaps between (b) and (d)). Overlap percentages were numerically small, but included key network groups, particularly Default and Salience / Ventral Attention (Sal/VentAttn).

Table 1-1. Detailed protocol from the full study from which the present data derives.

Figure 6-1. Behavioral predictions from CPMs. Values indicate r_s and uncorrected, two-tailed *p*-values from Spearman's partial rank correlation, computed between predicted and observed behavioral scores, controlled for motion. The *p*-value corresponding to each r_s was found by transforming the correlation coefficients to Student's *t* values by the partialcorr.m function in (*MATLAB*, 2014). Degrees of freedom for these tests were 66 for Models A and C, and 61 for Models B and D. (For AABresid, these *d.f.* values were 2 lower.) Note that all task scores had been re-oriented so that larger values indicate better task performance.

Figure 6-2. CPM predictions for models trained with VAB functional connectivity and behavioral data (Model types A and B) across edge selection thresholds. Within each subplot, the y-axis represents Spearman's rank correlation values, r_s, computed between predicted and observed task performance, controlled for motion. Horizontal gray lines indicate the corresponding p = .01, .05, .10, .10, .05, .01 (top to bottom) uncorrected levels of significance from standard r-to-p conversions, $d.f.$ = 71 (69 for AAB). The x-axis represents edge selection thresholds, $r_{threshold}$. The vertical gray line indicates the $r_{threshold}$ at the p = .05 level of significance, $d.f.$ = 70 (68 for AAB) due to one left-out participant during training. X-axis labels at the top of each plot indicate the average number of edges selected across all leave-one-out iterations at the corresponding $r_{threshold}$ on the bottom x-axis.

Figure 6-3. CPM predictions for models trained from task-specific behavioral data (Model types C and D) across edge selection thresholds. Within each subplot, the y-axis represents Spearman's rank correlation values, r_s, computed between predicted and observed task performance, controlled for motion. Horizontal gray lines indicate the corresponding p = .01, .05, .10, .10, .05, .01 (top to bottom) uncorrected levels of significance from standard r-to-p conversions, $d.f.$ = 71 (69 for AAB). The x-axis represents edge selection thresholds, $r_{threshold}$. The vertical gray line indicates the $r_{threshold}$ at the p = .05 level of significance, $d.f.$ = 70 (68 for AAB) due to one left-out participant during training. X-axis labels at the top of each plot indicate the average number of edges selected across all leave-one-out iterations at the corresponding $r_{threshold}$ on the bottom x-axis.

Figure 6-4. Permutation results of predicting VABresid data from VAB FC information, using the vabCPM (Model type A). The black line indicates Spearman's rank correlation values (r_s) computed between predicted and observed task performance, controlled for motion. Horizontal gray lines indicate the corresponding p = .01, .05, .10, .10, .05, .01 (top to bottom) uncorrected levels of significance from standard r-to-p conversions, based on N = 73. Green sections indicate p < .05 level of significance from permutation testing. Magenta sections indicate $p \geq .05$ level of significance from permutation testing. Our analysis demonstrates a high level of consistency in the significance of r_s values between using standard r-to-p conversions (black line) and using permutation testing (green/magenta line) for the majority of edge selection thresholds.

Figure 7-1. Results of applying the saCPM model to data in the present study. Values indicate r_s and uncorrected, two-tailed p-values from Spearman's rank correlation, computed between predicted and observed behavioral scores. The p-value corresponding to each r_s was found using standard r-to-p conversions, with $d.f.$ = 71 (69 for AABresid). All task scores had been re-coded so that larger values indicate better task performance.

Figure 8-1. Percentage of edge overlap for positive network edges between each pair of models. The value within each cell indicates the percentage of overlap between the pair of models on the corresponding x and y axes. Overlaps between the vabCPM (saCPM) with the other models are illustrated in the column (row) bounded in the red (black) of each plot. Axes labels also reflect the FC-Task pair used for training the task-specific model.

Figure 8-2. Percentage of edge overlap for negative network edges between each pair of models. The value within each cell indicates the percentage of overlap between the pair of models on the corresponding x and y axes. Overlaps between the vabCPM (saCPM) with the other models are illustrated in the column (row) bounded in the red (black) of each plot. Axes labels also reflect the FC-Task pair used for training the task-specific model.

Figure 8-3. Percentage of edge overlap between negative network (y-axis) and positive network (x-axis) edges. The value within each cell indicates the percentage of overlap between the pair of models on the corresponding x and y axes. Overlaps between the vabCPM (saCPM) with the other models are illustrated in the column (row) bounded in the red (black) of each plot. Axes labels also reflect the FC-Task pair used for training the task-specific model.

Figure 8-4. Percentage of edge overlap between positive network (y-axis) and negative network (x-axis) edges. The value within each cell indicates the percentage of overlap between the pair of models on the corresponding x and y axes. Overlaps between the vabCPM (saCPM) with the other models are illustrated in the column (row) bounded in the red (black) of each plot. Axes labels also reflect the FC-Task pair used for training the task-specific model.

1429 **Extended Data**

1430 Table 1-1. Detailed protocol from the full study from which the present data derives.

Session	Tasks/ Questionnaires	Session Description	Session Dur (hr)
1	Visual Attentional Blink (VAB) task	Participants were briefed on the study protocol in the first session and completed a target-probe Attentional Blink (AB) task to obtain a measure of baseline performance. Participants were only eligible to continue with the subsequent sessions if they obtained an average of 75% and above for target discrimination accuracy in the first session. Participants were not informed about their performance until the end of all experimental sessions.	1
2	Visual AB and surprise-induced blindness (SiB) task (in-scanner) Short-Sleep Questionnaire Visual Sustained Attention to Response task (12 mins) Attentional Network Task (30 mins) Theories of Intelligence Questionnaire	Participants had to return to the laboratory for the second session 3 to 14 days after the first session. The second session consisted of a 1.5 hr long fMRI scan. Task order was fixed across participants. No time limit was imposed on any of the questionnaires so participants could complete them at their own pace. All questionnaires were administered online using Qualtrics (Qualtrics, 2005).	2.5
3	Gradual-onset continuous Performance Task (15 mins)	The third session took place the day after the second session. Task order for the first 3 tasks was counterbalanced	2

	Auditory Sustained Attention to Response task (12 mins) Auditory AB and Surprise-induced deafness (SiD) task Visual AB task Visual AB task with colour-salient training	across participants.	
4	Visual AB and SiB task Visual Sustained Attention to Response task (12 mins) Attentional Network Task (30 mins) Adult ADHD Self-Report Scale Questionnaire Online Dimensional Change Card Sorting (DCCS) task Raven's Progressive Matrices Loss Aversion task	The fourth session took place the day after the third session. The Raven's Progressive Matrices task was an adapted version of the actual task that only consisted of 9 questions with no time limit given. Task order was fixed across participants.	2
5	Gradual-onset continuous Performance Task (15 mins) Auditory Sustained Attention to Response task (12 mins) Auditory AB and Surprise-	The fifth session took place the day after the fourth session. Decision-making tasks included a cups task and an explore-exploit task. Task order for the first three computerized tasks and questionnaires were counterbalanced and randomized across participants.	2

	induced deafness (SiD) task		
	Media-Multitasking Video Game Questionnaire		
	Personality Inventory for DSM-5 for adults		
	Wender Utah Rating Scale		
	Musical background and experience questionnaire		
	Decision-making tasks		
	Demographic Questionnaire		
6	Visual AB and surprise-induced blindness (SiB) task (in-scanner)	Session 6 was held between 5 to 14 days from the second session and consisted of a 1.5 hr long fMRI scan that used a protocol identical to that of the first in-scanner session so as to investigate test-retest reliability. Participants were encouraged to take breaks between experimental blocks and between tasks to alleviate fatigue.	1.5

1431

Figure 6-1. Behavioral predictions from CPMs. Values indicate r_s and uncorrected, two-tailed *p*-values from Spearman's partial rank correlation, computed between predicted and observed behavioral scores, controlled for motion. The *p*-value corresponding to each r_s was found by transforming the correlation coefficients to Student's *t* values by the partialcorr.m function in (*MATLAB*, 2014). Degrees of freedom for these tests were 66 for Models A and C, and 61 for Models B and D. (For AABresid, these *d.f.* values were 2 lower.) Note that all task scores had been re-oriented so that larger values indicate better task performance.

Task domain	Train	Model A VABFC-VABresid		Model B VABFC-VABresid		Model C VABFC-Task		Model D RSFC-Task	
	Test	VABFC-Task		RSFC-Task		VABFC-Task		RSFC-Task	
	Task	r_s	*p*	r_s	*p*	r_s	*p*	r_s	*p*
Attentional Blink	VABresid	0.308	0.011*	0.123	0.338	0.308	0.011*	0.148	0.228
	AABresid	0.04	0.748	-0.107	0.411	0.135	0.279	-0.053	0.672
Sustained Attention	VSARTdprime	-0.268	0.027*	-0.19	0.135	0.245	0.044*	0.062	0.617
	ASARTdprime	-0.062	0.617	-0.212	0.096	-0.021	0.866	0.201	0.1
	GradCPTdprime	0.058	0.637	-0.097	0.451	-0.265	0.029*	0.226	0.063
Selective Attention	ANTerr	-0.33	0.006*	-0.308	0.014*	0.346	0.004*	0.14	0.256
	ANTrtvar	-0.36	0.003*	-0.414	0.001*	0.24	0.049*	0.232	0.057
	ANTaert	0.051	0.682	0.141	0.269	0.033	0.787	-0.061	0.619
	ANToert	0.063	0.609	0.128	0.318	0.124	0.313	0.032	0.793
	ANTcert	-0.252	0.038*	-0.333	0.008*	0.032	0.798	0.262	0.031*
Fluid Intelligence	RavensAcc	0.245	0.044*	0.224	0.077	-0.125	0.31	0.374	0.002*

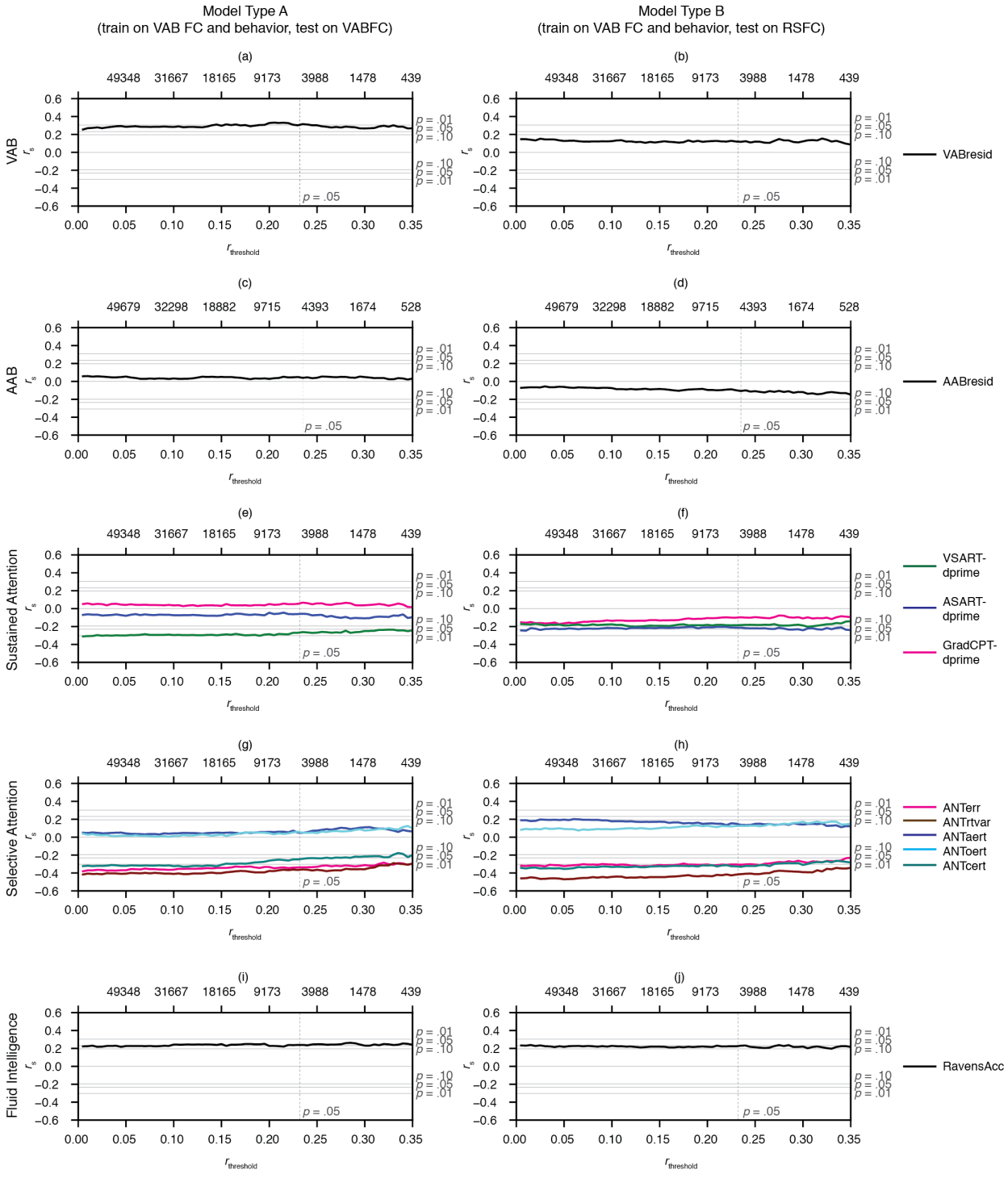

1440

1441 Figure 6-2. CPM predictions for models trained with VAB functional connectivity and

1442 behavioral data (Model types A and B) across edge selection thresholds. Within each subplot, the

y-axis represents Spearman's rank correlation values, r_s, computed between predicted and observed task performance, controlled for motion. Horizontal gray lines indicate the corresponding p = .01, .05, .10, .10, .05, .01 (top to bottom) uncorrected levels of significance from standard r-to-p conversions, $d.f.$ = 71 (69 for AAB). The x-axis represents edge selection thresholds, $r_{threshold}$. The vertical gray line indicates the $r_{threshold}$ at the p = .05 level of significance, $d.f.$ = 70 (68 for AAB) due to one left-out participant during training. X-axis labels at the top of each plot indicate the average number of edges selected across all leave-one-out iterations at the corresponding $r_{threshold}$ on the bottom x-axis.

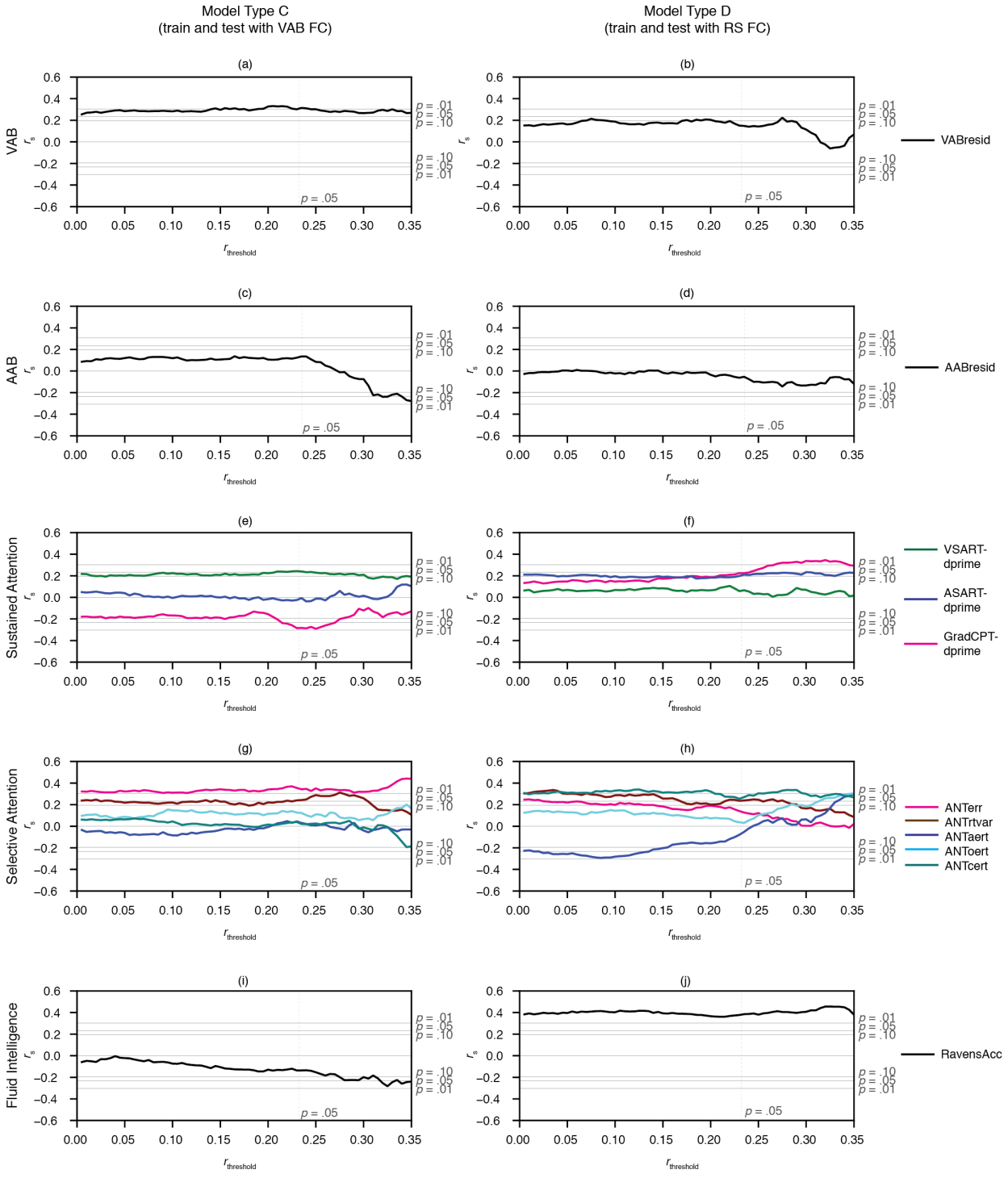

1451

1452 Figure 6-3. CPM predictions for models trained from task-specific behavioral data (Model types

1453 C and D) across edge selection thresholds. Within each subplot, the y-axis represents Spearman's

rank correlation values, r_s, computed between predicted and observed task performance, controlled for motion. Horizontal gray lines indicate the corresponding p = .01, .05, .10, .10, .05, .01 (top to bottom) uncorrected levels of significance from standard r-to-p conversions, $d.f.$ = 71 (69 for AAB). The x-axis represents edge selection thresholds, $r_{threshold}$. The vertical gray line indicates the $r_{threshold}$ at the p = .05 level of significance, $d.f.$ = 70 (68 for AAB) due to one left-out participant during training. X-axis labels at the top of each plot indicate the average number of edges selected across all leave-one-out iterations at the corresponding $r_{threshold}$ on the bottom x-axis.

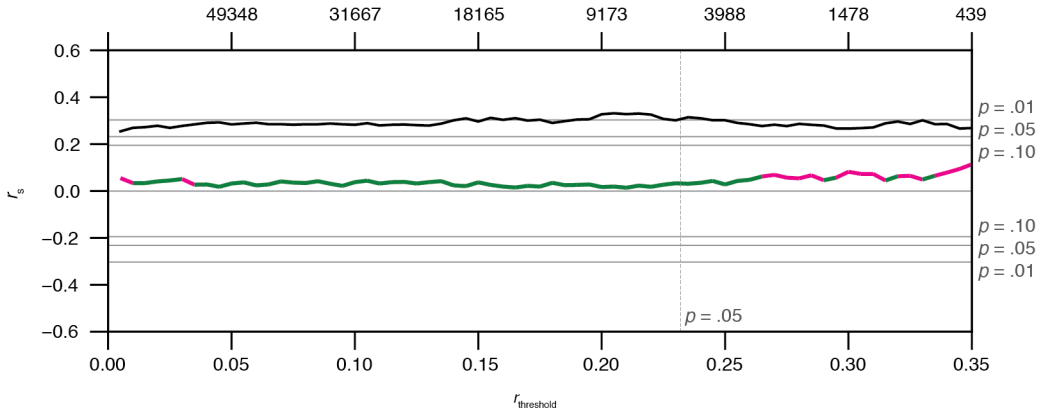

Figure 6-4. Permutation results of predicting VABresid data from VAB FC information, using the vabCPM (Model type A). The black line indicates Spearman's rank correlation values (r_s) computed between predicted and observed task performance, controlled for motion. Horizontal gray lines indicate the corresponding p = .01, .05, .10, .10, .05, .01 (top to bottom) uncorrected levels of significance from standard r-to-p conversions, based on N = 73. Green sections indicate p < .05 level of significance from permutation testing. Magenta sections indicate $p \geq .05$ level of significance from permutation testing. Our analysis demonstrates a high level of consistency

in the significance of r_s values between using standard *r*-to-*p* conversions (black line) and using permutation testing (green/magenta line) for the majority of edge selection thresholds.

Figure 7-1. Results of applying the saCPM model to data in the present study. Values indicate r_s and uncorrected, two-tailed *p*-values from Spearman's rank correlation, computed between predicted and observed behavioral scores. The *p*-value corresponding to each r_s was found using standard *r*-to-*p* conversions, with *d.f.* = 71 (69 for AABresid). All task scores had been re-coded so that larger values indicate better task performance.

Task domain	Task	saCPM (VABFC)		saCPM (RSFC)	
		r_s	*p*	r_s	*p*
Attention Blink	VABresid	-0.235	0.045*	-0.155	0.191
	AABresid	0.049	0.684	-0.132	0.271
Sustained Attention	VSARTdprime	0.278	0.018*	0.271	0.021*
	ASARTdprime	0.117	0.323	0.290	0.013*
	GradCPTdprime	0.027	0.822	0.086	0.469
Selective Attention	ANTerr	0.322	0.005*	0.156	0.189
	ANTrtvar	0.329	0.005*	0.270	0.021*
	ANTaert	-0.057	0.629	-0.099	0.405
	ANToert	-0.101	0.397	-0.155	0.190
	ANTcert	0.224	0.057	0.384	0.001*
Fluid Intelligence	RavensAcc	-0.059	0.620	-0.229	0.052

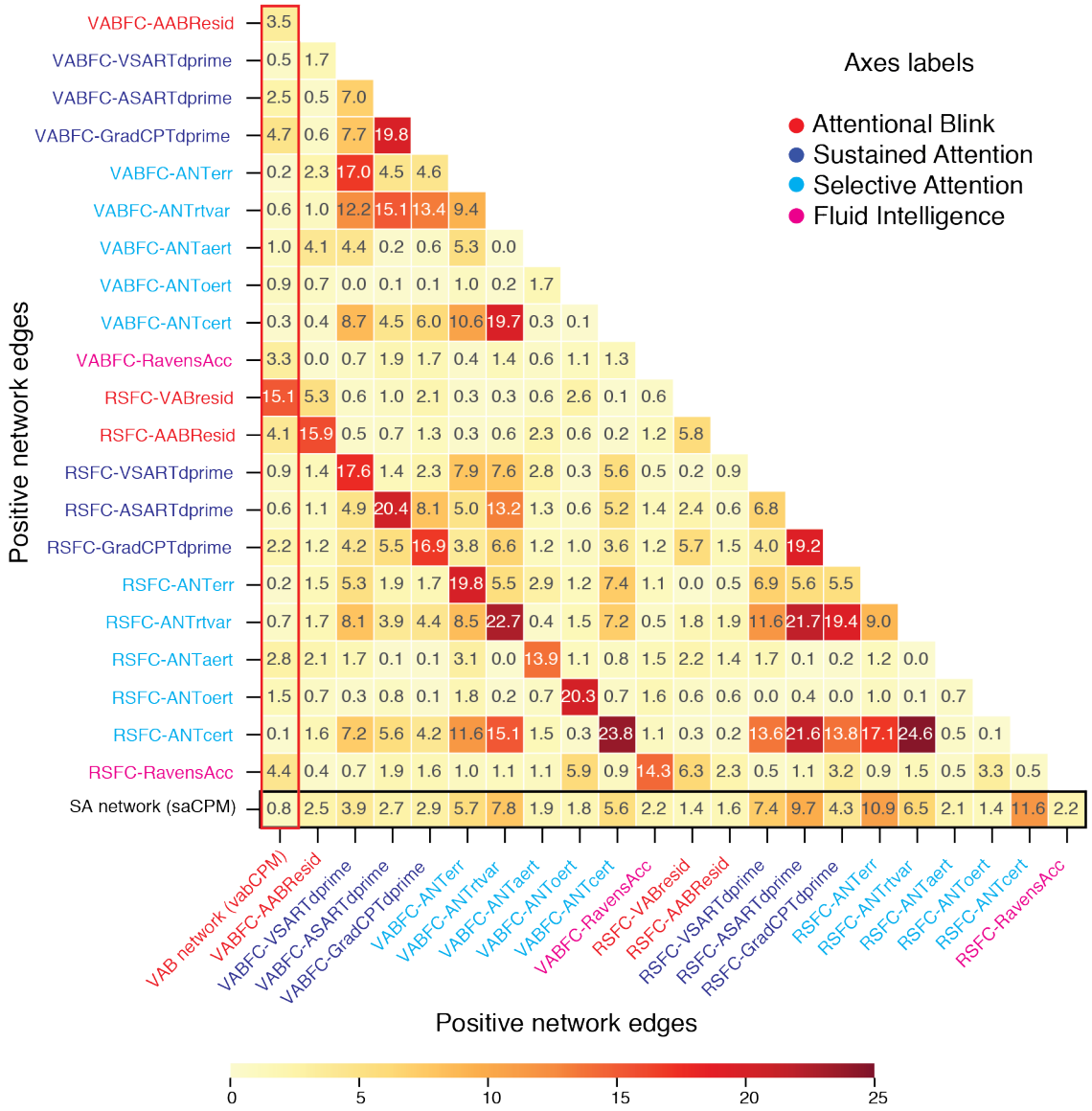

1480

1481 Figure 8-1. Percentage of edge overlap for positive network edges between each pair of models.

1482 The value within each cell indicates the percentage of overlap between the pair of models on the

1483 corresponding x and y axes. Overlaps between the vabCPM (saCPM) with the other models are

1484 illustrated in the column (row) bounded in the red (black) of each plot. Axes labels also reflect

1485 the FC-Task pair used for training the task-specific model.

1486

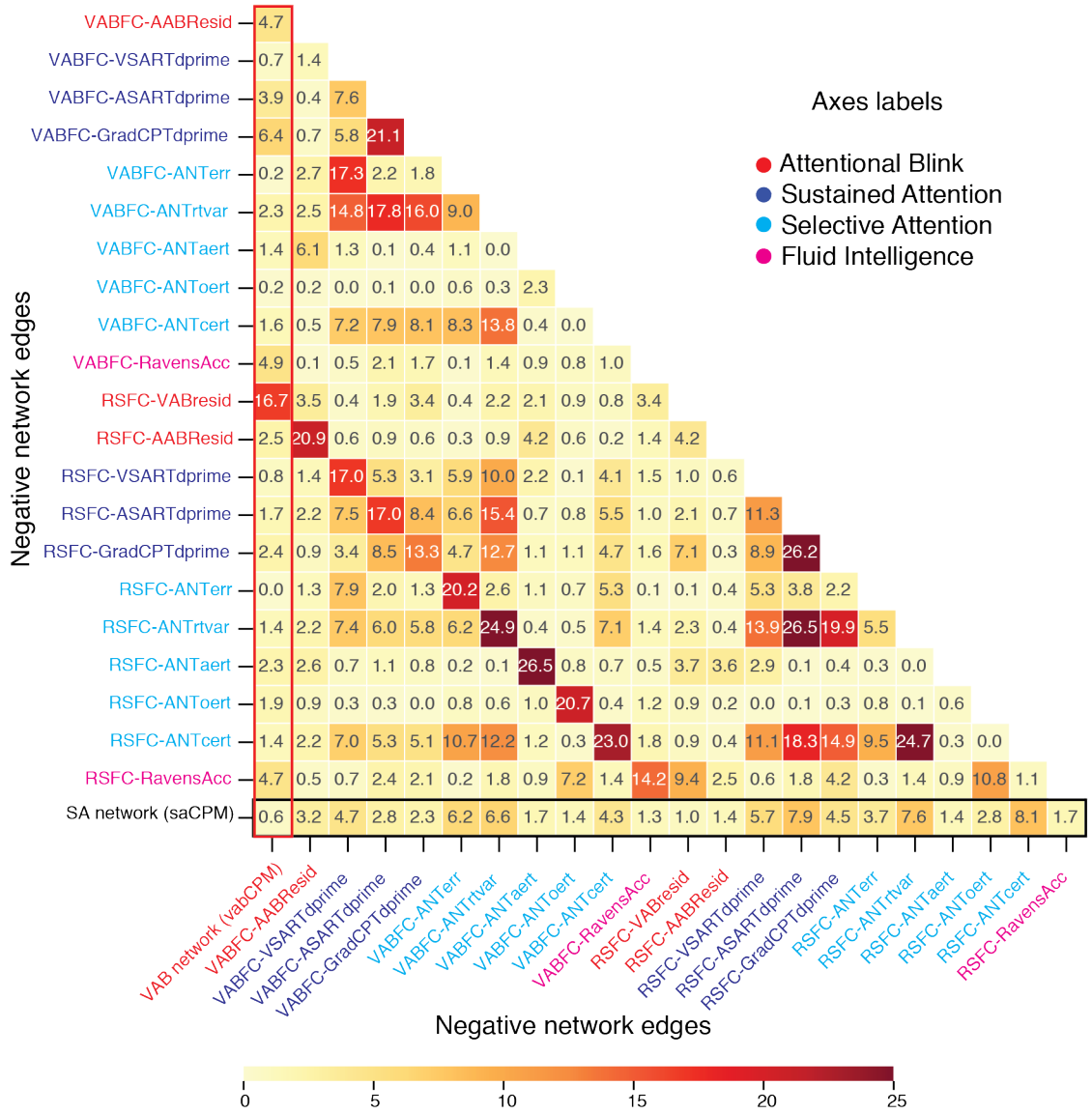

1487

1488 Figure 8-2. Percentage of edge overlap for negative network edges between each pair of models.

1489 The value within each cell indicates the percentage of overlap between the pair of models on the

1490 corresponding x and y axes. Overlaps between the vabCPM (saCPM) with the other models are

1491 illustrated in the column (row) bounded in the red (black) of each plot. Axes labels also reflect

1492 the FC-Task pair used for training the task-specific model.

1493

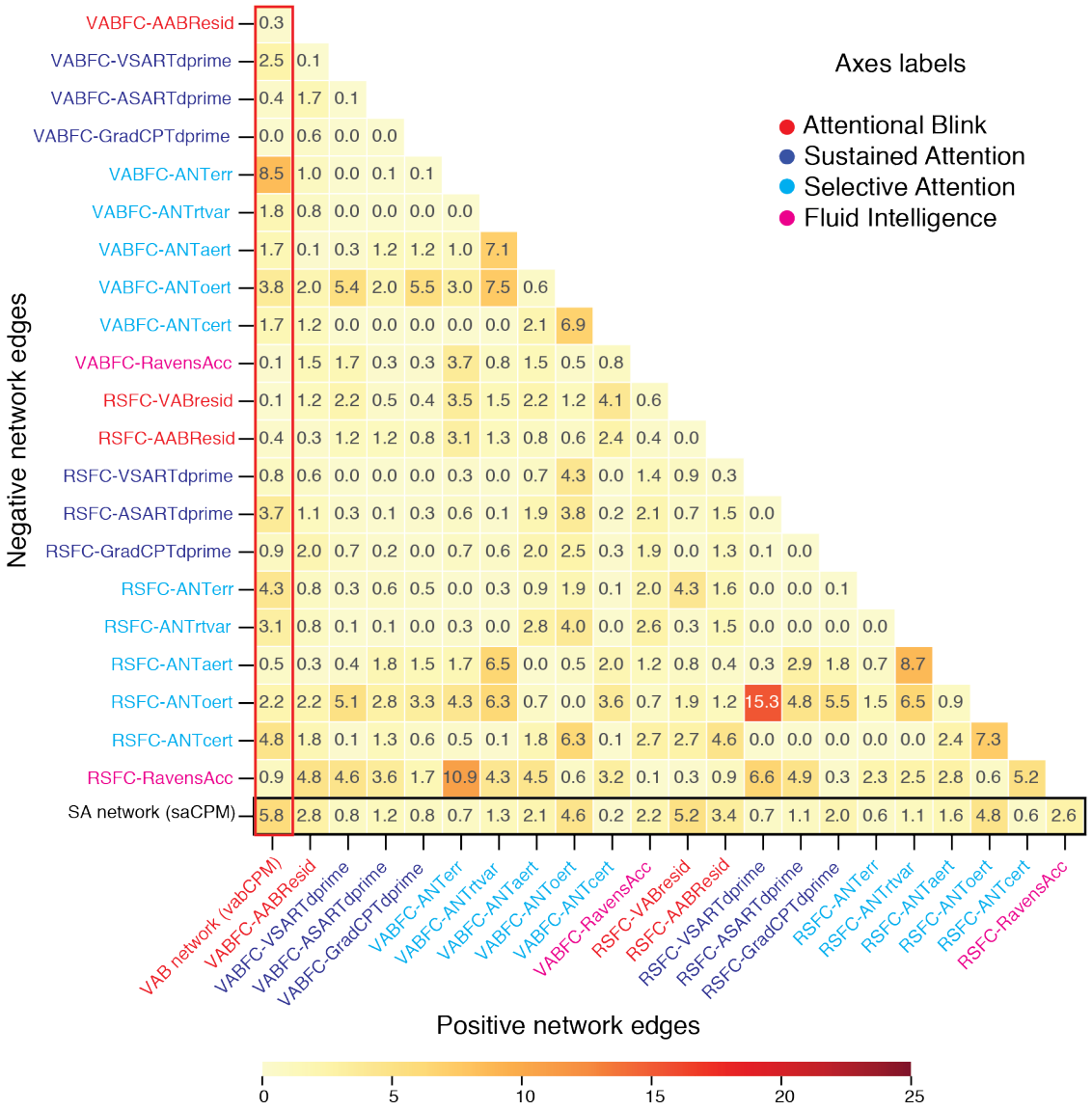

Figure 8-3. Percentage of edge overlap between negative network (y-axis) and positive network (x-axis) edges. The value within each cell indicates the percentage of overlap between the pair of models on the corresponding x and y axes. Overlaps between the vabCPM (saCPM) with the other models are illustrated in the column (row) bounded in the red (black) of each plot. Axes labels also reflect the FC-Task pair used for training the task-specific model.

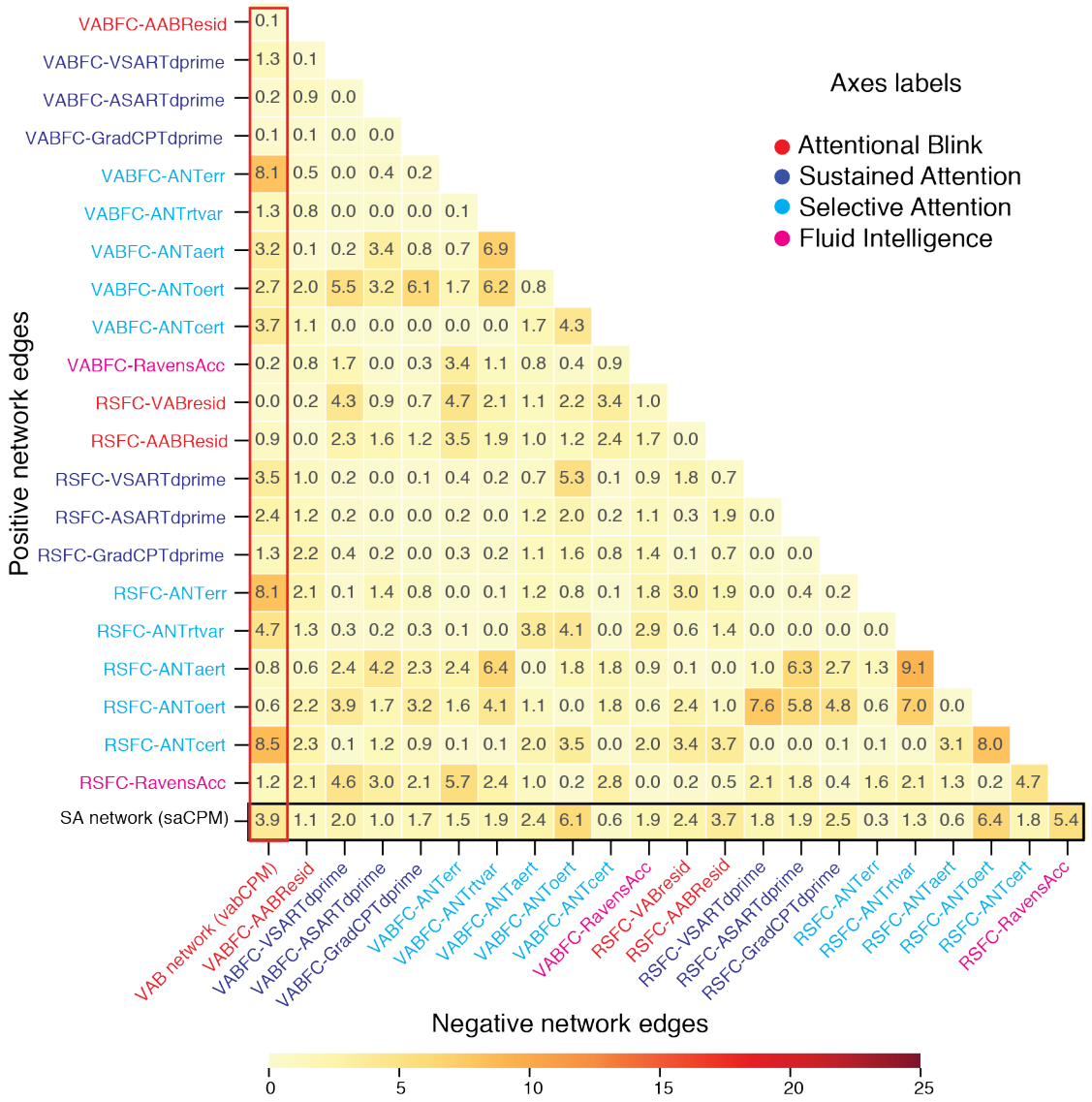

1501

1502 Figure 8-4. Percentage of edge overlap between positive network (y-axis) and negative network

1503 (x-axis) edges. The value within each cell indicates the percentage of overlap between the pair of

1504 models on the corresponding x and y axes. Overlaps between the vabCPM (saCPM) with the

1505 other models are illustrated in the column (row) bounded in the red (black) of each plot. Axes

1506 labels also reflect the FC-Task pair used for training the task-specific model.

1507